

# From Accurate Quantum Chemistry to Converged Thermodynamics for Ion Pairing in Solution

Niamh O'Neill,<sup>1,2,3,4</sup> Benjamin X. Shi,<sup>5</sup> William C. Witt,<sup>6</sup> Blake I. Armstrong,<sup>7</sup> William J. Baldwin,<sup>3,8</sup> Paolo Raiteri,<sup>7</sup> Christoph Schran,<sup>2,3,\*</sup> Angelos Michaelides,<sup>1,3,†</sup> and Julian D. Gale<sup>7,‡</sup>

<sup>1</sup>*Yusuf Hamied Department of Chemistry, University of Cambridge, Lensfield Road, Cambridge, CB2 1EW, UK*

<sup>2</sup>*Cavendish Laboratory, Department of Physics, University of Cambridge, Cambridge, CB3 0HE, UK*

<sup>3</sup>*Lennard-Jones Centre, University of Cambridge, Trinity Ln, Cambridge, CB2 1TN, UK*

<sup>4</sup>*Max Planck Institute for Polymer Research, Mainz 55128, Germany*

<sup>5</sup>*Initiative for Computational Catalysis, Flatiron Institute, 160 5th Avenue, New York, NY 10010, USA*

<sup>6</sup>*Harvard John A. Paulson School of Engineering and Applied Sciences, Harvard University, Cambridge, MA, USA*

<sup>7</sup>*School of Molecular and Life Sciences, Curtin University,  
PO Box U1987, Perth, Western Australia 6845, Australia*

<sup>8</sup>*Engineering Department, Trumpington St, Cambridge CB2 1PZ, UK*

Quantitative prediction of thermodynamic properties in solution is essential for translating atomistic simulations into reliable chemical insight. As an exemplar system, the behaviour of  $\text{CaCO}_3$  in water has been widely studied to understand its mineralization in seawater, with potential implications for carbon-capture strategies. However, making accurate computational predictions has been a long-standing challenge, requiring both highly accurate electronic structure methods and extensive statistical sampling. Here, we combine advances in machine learning and electronic structure theory to fully resolve the ion pairing free energy of  $\text{CaCO}_3$  with explicit solvation. We show that achieving quantitative agreement with experiment requires going beyond the standard density functional theory up to the “gold-standard” coupled cluster theory with single, double, and perturbative triple excitations [CCSD(T)]. We generate a set of systematically improvable models, enabling reliable insights into the initial association mechanism of Ca and  $\text{CO}_3$  ions prior to nucleation while fully quantifying enthalpic and entropic effects. Our results demonstrate that CCSD(T)-level thermodynamic predictions of complex aqueous systems can now be routinely achieved.

## INTRODUCTION

Ions in solution play central roles in processes ranging from biomolecular function and mineralization [1] to energy storage and conversion technologies [2]. As an archetypal example, calcium carbonate ( $\text{CaCO}_3$ ) is a crucial ionic species in seawater, which – upon mineralisation – forms the primary structural component of geological structures such as coral reefs [3] and serves as a promising route for long-term carbon sequestration [4, 5]. More fundamentally, it is often used as a model system for nucleation theories [6]. However the molecular mechanism of ion pairing and its relationship to nucleation remains poorly understood, despite sustained experimental and computational investigation [1, 7–14]. A major reason for this is that the macroscopic phenomena of mineralisation and dissolution are ultimately governed by the highly delicate nature of the interactions between individual ions and their aqueous solvation environment. Since these interactions are difficult to probe directly in experiments, atomistic simulations can provide a powerful framework to link microscopic structure to macroscopic behaviour [15].

The fundamental property of interest for  $\text{CaCO}_3$ , and most ions, is the ion pair association free energy in solution. It can be measured experimentally and serves as a stringent benchmark for assessing the reliability of atomistic insights obtained from simulations. However, accurately predicting this quantity is challenging [16]. First, it requires a faithful description of the underlying potential

energy surface (PES), governed by a delicate balance of ion–ion, ion–water, and water–water interactions. Second, reliable estimates demand thorough sampling of this PES to capture finite-temperature and entropic contributions [17]. In practice, enhanced sampling methods are needed to efficiently explore multiple ion pairing minima within accessible simulation timescales. Finally, the solvent must be modeled explicitly to account for its effects both on the PES and the thermodynamic sampling.

These stringent requirements, illustrated here for  $\text{CaCO}_3$ , form the central challenge for any atomistic simulation in solution. Classical force fields are computationally efficient but often insufficiently accurate, whereas first-principles (*ab initio*) methods may be more accurate but the concurrent sampling demands make it too costly for well-converged *ab initio* molecular dynamics (AIMD) simulations. Machine learning potentials (MLPs) have emerged as a promising strategy to bridge this gap, training surrogate models to reproduce first-principles methods at significantly reduced cost. It has become routine to train MLPs to density functional theory (DFT), the workhorse first-principles method, with notable success achieved across diverse systems, including  $\text{CaCO}_3$  [18]. The efficiency of computing DFT energies and gradients, together with mature implementations of periodic boundary conditions to describe the condensed phase, has enabled relatively standardized protocols for fitting DFT-level MLPs. However, the accuracy of the resulting MLP is ultimately limited by the underlying density functional approximation (DFA). In particular, delocalization error [19]

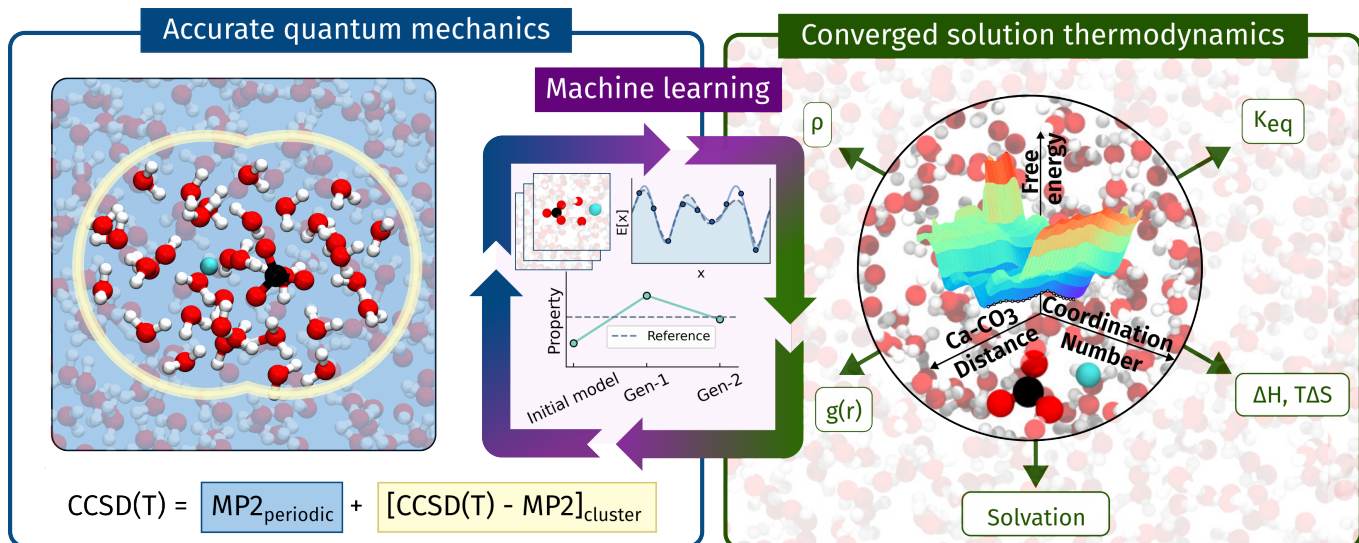


**Figure 1: Workflow combining accurate electronic structure, MLPs and enhanced sampling:** Schematic of the framework used in this work, using MLPs to access converged thermodynamics in solution at various levels of electronic structure theory. To obtain the CCSD(T) level model a  $\Delta$ -learning approach uses gas phase clusters to correct the periodic MP2 model to CCSD(T) level. In general the models are ‘self-consistently’ converged to ensure reliable predictions of the density and PMF (generically labelled ‘Property’ in the middle panel) and adequate sampling of configuration space. Finally efficient implementations of the MLPs are used in tandem with enhanced sampling simulations to resolve the thermodynamics of complex potential (free) energy surfaces.

– especially problematic for charged anions [20–22] – can lead to qualitatively incorrect densities and solvation structures [23, 24]. For example, a recent MLP trained to the SCAN functional surpasses many force-fields in describing  $\text{CaCO}_3$  from aqueous solution to the solid state [18], but its predicted ion pair association free energy remains several kJ/mol from experiment.

Correlated wavefunction theory (cWFT) on the other hand, provides a systematically improvable hierarchy of methods. The random phase approximation (RPA) and second-order Møller–Plesset perturbation theory (MP2) form the lower tiers of this hierarchy, and often improve the description of ions over DFT as they naturally capture van der Waals interactions [23, 25] while mitigating delocalization error. Periodic implementations of RPA [26] and MP2 [27, 28] that also compute gradients are now mature enough to train MLPs using strategies similar to those developed for DFT [23]. However, achieving quantitative accuracy with these methods is still challenging. For example MP2 significantly overestimates the density of water [29, 30], while RPA tends to underestimate lattice energies of ice [31]. The method of choice – the “gold standard” – is coupled cluster theory with single, double, and perturbative triple excitations [CCSD(T)], which has demonstrated reliable accuracy across diverse material and molecular systems [32–39]. However, its steep computational cost – formally scaling as  $N^7$  with  $N$  electrons – along with the lack of mature periodic and gradient implementations, makes CCSD(T) impractical for routine molecular dynamics simulations and incompatible with standard DFT-based MLP training strategies.

Nevertheless, there have been several approaches that aim to achieve CCSD(T)-level accuracy in finite-temperature simulations of condensed-phase aqueous systems. One strategy uses a multi-level approach, in an embedding-style scheme, which starts from a simulation at a lower level of theory and applies CCSD(T) corrections to localized regions [40, 41]. The most advanced study to date explored pH effects on Ca (and Mg) ion hydration, combining DFT-based biased AIMD simulations with quantum embedding of selected fragments [42]. While these methods can achieve high accuracy, extending them to processes such as ion pairing and beyond, where multiple interacting regions may be involved, is not straightforward. Additionally, such an approach only corrects the internal energy, and so the effect on the entropic contribution to the free energy from different levels of theory remains an open question.

Alternative approaches aim to directly parameterise the CCSD(T) PES to be directly sampled during simulations. One highly successful family of approaches is based on the many-body expansion, with MB-pol achieving excellent agreement with experiment for hydration properties of simple alkali and halide ions in water [43–45] while q-AQUA-pol also accurately reproduces bulk water properties [46]. Most recent is the development of CCSD(T)-level MLPs to directly model the condensed phase PES [47–49]. In particular,  $\Delta$ -learning targets the CCSD(T) correction to DFT in the condensed phase by extrapolating from gas-phase clusters, alleviating the aforementioned limitations with periodic CCSD(T). Although successful for liquid water [47–49] and gas phase molecular systems [50], extending these strategies to more complex multicomponent systems in the condensed

phase remains a major challenge.

In this work, we generalize our recently proposed  $\Delta$ -learning framework for liquid water [49] to study ions in solution with CCSD(T)-level MLPs, using the ion pairing of  $\text{CaCO}_3$  as a case study system. As illustrated in Figure 1, we leverage recent advances in efficient periodic MP2 implementations [28] to construct a baseline MLP trained at the MP2 level. A separate  $\Delta$ -MLP is then trained to learn the MP2-to-CCSD(T) correction using gas-phase clusters (centred on both ions) extracted from the periodic configurations. The final CCSD(T) MLP is the sum of (energies and forces) predicted by the baseline and  $\Delta$ -MLPs as illustrated in the left-hand panel of Figure 1. The underlying periodic dataset and derived  $\Delta$ -dataset are improved iteratively to converge the potential of mean force (PMF) used to compute the ion pair binding free energy, ensuring reliable prediction of the thermodynamic properties (illustrated in the centre panel of Figure 1). Further details on the model training and validation are given in Section 1 of the Supplementary Information (SI).

Combining our CCSD(T) MLP model with state-of-the-art enhanced sampling approaches [51], we achieve excellent agreement with experimental values for the ion pair association free energy of  $\text{CaCO}_3$  in water. It must be emphasized here that this approach enables the entire PES and thermodynamic sampling to be explicitly treated at the CCSD(T) level. We decompose the ion pairing free energy into its enthalpic and entropic contributions, and compare to MLP models trained to several DFT functionals, as well as RPA and MP2. We show that the CCSD(T) model is the only model that simultaneously agrees with experiment for the free energy, enthalpy and entropy, indicating also that the correct answer requires converged interactions. With the CCSD(T) model validated, we provide atomistic insights into the binding mechanism of  $\text{CaCO}_3$  in water, highlighting salient differences in the mechanism between levels of theory. Overall, this work shows that thermodynamics of complex aqueous systems at cWFT accuracy – and in particular at the CCSD(T) level – is now accessible, opening a route towards routine, high-accuracy simulations of experimentally relevant processes in solution.

### AGREEMENT WITH EXPERIMENT ON $\text{CaCO}_3$ ION PAIRING

We begin by considering ion pairing free energies at 300 K ( $\Delta G_{300\text{K}}$ ), as shown in the top panel of Figure 2. Reported in the figure are experimental measurements and values obtained from MLPs trained at increasing levels of electronic structure theory and computed with on-the-fly probability enhanced sampling (OPES) [51]. Two experimental values are available, depending on the speciation model used to interpret the data [52, 53] and cover a range of 4 kJ/mol (the range of chemical accuracy). We compare models trained in this work at the DFT level (revPBE-D3 [54, 55] and

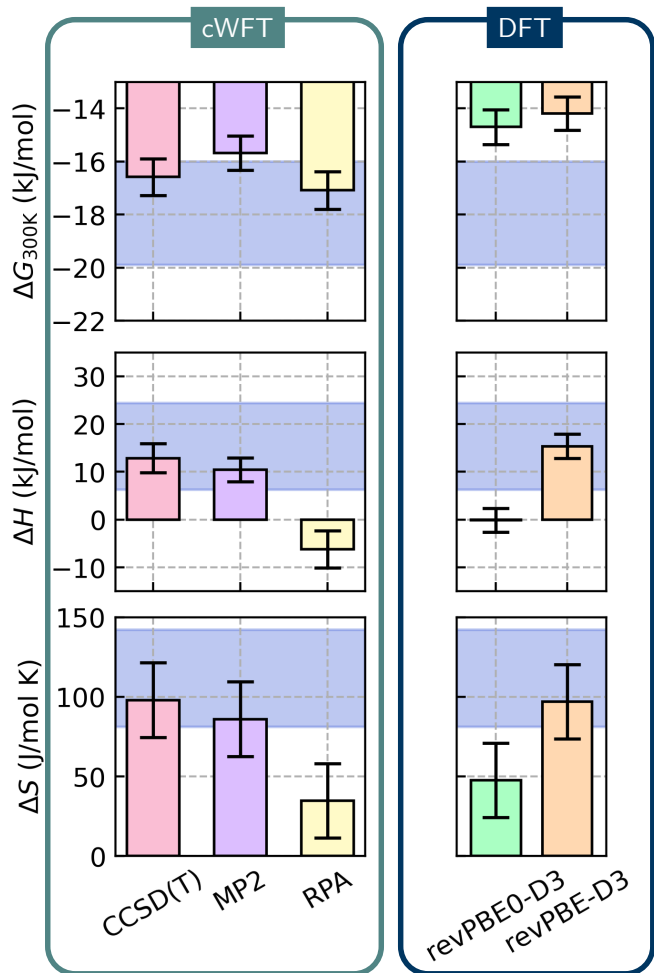


**Figure 2: Ion pair association free energy, enthalpy and entropy from OPES simulations:** Comparison of cWFT MLPs (CCSD(T), MP2 and RPA) and DFT MLPs (revPBE0-D3, revPBE-D3) for (top) the standard ion pair association free energy at 300 K (middle) enthalpy and (bottom) entropy of ion pair association. The experimental range from literature [52, 53] is shaded in blue for each quantity. Error bars on the cWFT and DFT results are the standard error on the mean of 6 independent OPES simulations. All results have also been corrected for finite size effects, as described in Section 10 of the SI. Convergence of the OPES simulations is also shown in Figure 6 of the SI, as well as the full temperature dependence of the ion pair association free energy used to obtain the enthalpy and entropy in Figure 7 of the SI.

revPBE0-D3 [56, 57]), as well as RPA, MP2, and CCSD(T). The predicted binding free energies span a range of roughly 3 kJ/mol. A clear trend emerges: agreement with experiment improves with increasing level of theory. In particular, the RPA-, MP2-, and CCSD(T)-based models achieve quantitative agreement with experiment for  $\Delta G_{300\text{K}}$ . By contrast, the widely used GGA functional revPBE-D3 underestimates the binding free energy. Although hybrid DFT has been suggested to improve charge localization and the relative stability of contact and solvent-shared ion pairs [13, 17],

revPBE0-D3 shows little improvement over revPBE-D3 and still underestimates the binding strength.

The real challenge emerges in Figures 2b and 2c, which highlight the difficulty of accurately capturing the delicate balance of enthalpy and entropy underlying the ion pairing. These contributions differentiate the models, showing that while some can reproduce the free energy at 300 K, this is only through fortuitous error cancellation. For example, although RPA yields the correct ion pairing free energy at 300 K, it predicts a negative enthalpy and a significantly underestimated entropy compared to experiments. Conversely, revPBE-D3 reproduces the experimental enthalpy and entropy but underestimates the 300 K free energy. Only CCSD(T) consistently agrees with experiment for the free energy, enthalpy, and entropy. These results emphasize the twofold requirement of an accurate cWFT-level PES and exhaustive sampling to properly capture entropic effects.

## RELIABLE CHEMICAL INSIGHTS INTO ION PAIRING MECHANISMS

Having established the quantitative accuracy of our CCSD(T) MLP, we now use it to examine the atomistic ion pairing pathways. The left panel of Figure 3 shows the two-dimensional (2D) free energy surface as a function of the Ca–CO<sub>3</sub> separation and Ca–O<sub>H<sub>2</sub>O</sub> coordination number (CN) for revPBE-D3, revPBE0-D3, and CCSD(T). The corresponding one-dimensional (1D) potential of mean force (PMF), obtained by integrating over the Ca–O<sub>H<sub>2</sub>O</sub> coordination number, is shown above each surface (with the other functionals shown in Figures 8 and 9 in the SI). In order of increasing ion – ion separation, the key states are the bidentate (1) and monodentate (2) contact ion pairs (CIPs), the solvent-shared ion pair (SShIP) (3), and the solvent-separated ion pair (SSIP) (4), illustrated above the 1D PMFs.

The 1D PMF now clarifies why revPBE-D3 and revPBE0-D3 – both widely used DFAs for aqueous systems – underestimate the 300 K binding free energy. Relative to CCSD(T) (as well as MP2 in Figure 8 of the SI), the two DFAs predict incorrect stabilities of the CIPs, with the bidentate and monodentate CIPs nearly isoenergetic. In contrast, CCSD(T) stabilizes the bidentate CIP significantly over the monodentate form. Both DFT methods also predict the opposite stability of the CIP states and SShIP relative to CCSD(T). The overstabilization of more separated states relative to the CIPs is consistent with delocalization error in DFT, which favors weaker ionic character. We also analyse the charges on the ions predicted by the different levels of theory (up to MP2) via Bader charge partitioning in Section 3 of the SI, which confirms increased localization at higher levels of theory. Physically, this aligns with prior force-field studies showing that larger ionic charges are necessary to achieve quantitative agreement with experiment [14].

Among the first-principles methods studied in this work,

only MP2 reproduces the CCSD(T) trend, although it slightly underestimates the depth of the CIP (shown in Figure 8 of the SI). The relative stabilities of the CIP and SShIP predicted by our MP2 model are also in quantitative agreement with previous literature [42], which corrects enthalpic contributions for specific features of a DFT free energy profile up to the MP2 level by applying quantum embedding to extracted fragments (see Figure 12 of the SI).

The 2D free energy surface further highlights distinct differences in the minimum energy path for ion pairing/dissociation between the different levels of theory. While CCSD(T) and revPBE0-D3 remain in the CIP state as the Ca–O<sub>H<sub>2</sub>O</sub> CN increases from 5 to 6 to 7, at each step, revPBE-D3 follows a different mechanism. It first increases the ion pair separation before adding further water molecules to its coordination shell, possibly arising from delocalisation error favouring more diffuse spread of charge. Furthermore, both revPBE-D3 and revPBE0-D3 show increased preference for lower coordination with water at large ion separations compared to CCSD(T), which more easily accommodates an additional water in the Ca solvation shell (and will be discussed in more detail in the next Section).

## RESOLVING ION SOLVATION STRUCTURE

We now focus on the hydration structure of the individual ions, showing the free energy as a function of Ca–O<sub>H<sub>2</sub>O</sub> (and CO<sub>3</sub>–O<sub>H<sub>2</sub>O</sub>) CN at 300 K in the right panel of Figure 3, obtained from simulations of the individual ions in water. Pinning down the hydration structure of the ions is highly challenging, with literature values for the Ca–O<sub>H<sub>2</sub>O</sub> CN ranging between 5 and 10 from different experiments [58–61] and a similar spread from simulations [62–66]. In this case, the accuracy of the underlying model, a limited sampling of the full free energy surface arising from only static 0 K calculations and the practical challenges to isolate individual ion-water interactions from experiments contribute to the large variability in predictions.

Our simulations show there is a wide range of accessible states for the Ca–O<sub>H<sub>2</sub>O</sub> CN predicted by all methods, where between 6-, 7-, 8- and 9-fold coordination states are all accessible. On the other hand, the CO<sub>3</sub>–O<sub>H<sub>2</sub>O</sub> profiles are much broader, with fewer discrete coordination states. We observe a shift towards lower coordination numbers of Ca with water for lower levels of theory, with a similar trend for CO<sub>3</sub>. This may be explained by the greater localization of charge for MP2 and CCSD(T) enabling stronger binding with the waters in the first solvation shell, with lower levels of theory having more diffuse charge environments around the ions.

These profiles again highlight the challenge of obtaining reliable atomistic insights to rationalise experiment from simulation when only considering 0 K properties, or alternatively the free energy but at a lower level of theory. The wide range of accessible states, coupled with the sensitive differ-

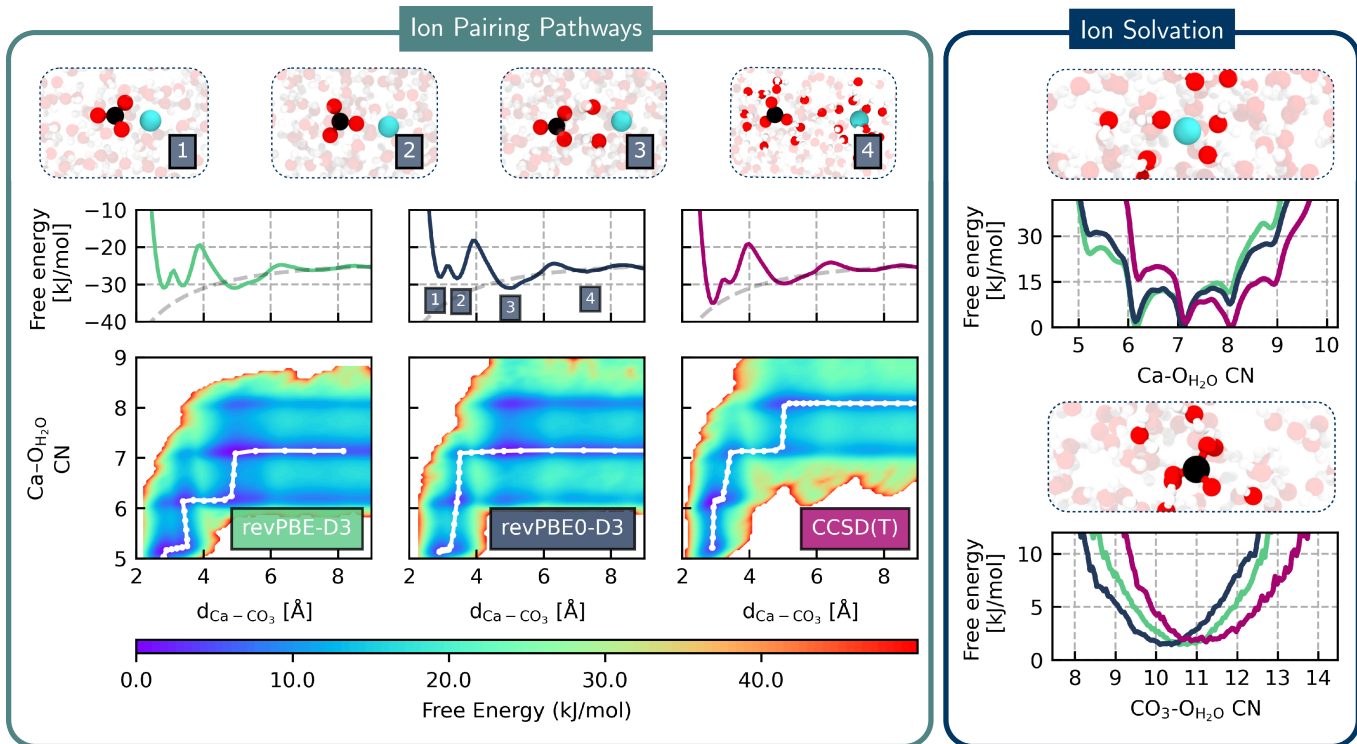


**Figure 3: CaCO<sub>3</sub> ion pair dissociation pathways and ion solvation:** Left panel: Ion pairing pathways for a selection of models at 300 K: revPBE-D3, revPBE0-D3 and CCSD(T). The minimum free energy path in each case is plotted in white. Above is the potential of mean force, aligned to the analytic solution for point charges in a dielectric medium (grey dashed line). The bidentate contact ion pair (1), monodentate contact ion pair (2), solvent-shared ion pair (3) and solvent separated ion pair (4) are labelled for the revPBE0-D3 case, along with representative snapshots above. In the snapshots, calcium, carbon, oxygen and hydrogen are coloured blue, green, red and white, respectively. Right panel: Free energy as a function of water coordination number for a calcium (top) and carbonate (bottom) ion in water for revPBE-D3, revPBE0-D3 and CCSD(T) models. Representative snapshots are shown alongside (only a small region of the full simulation cell is shown).

ences between levels of theory emphasise the importance of sampling the full free energy surface with a sufficiently accurate description of the electronic structure.

## DISCUSSION

Years of effort in the parameterisation of classical force-field models for CaCO<sub>3</sub> also achieve good experimental agreement for the ion pairing free energies, enthalpy, entropy and solvation structure [14] as shown in Figure 13 of the SI. Such models have been directly fitted to match experimental hydration free energies of the ions, (which is correlated to a large extent to the ion pairing association free energy), and so transferability is not guaranteed for more complex situations. On the other hand, our MLP-based framework provides a systematic path towards the correct solution, starting from MP2 and adding a correction to CCSD(T). Importantly, the models developed in this work require no additional empirical fitting parameters to achieve experimental agreement.

The value of this approach becomes more apparent when the steps beyond ion pairing are considered, where an accu-

rate model has been sorely needed to resolve open questions regarding the nucleation mechanism of CaCO<sub>3</sub>. In particular there is intense debate over possible non-classical mechanisms including liquid-liquid phase separation [67, 68], and transformation to the solid phase via thermodynamically stable pre-nucleation clusters [1, 8, 11, 12]. Alternative simulation work proposes that such clusters play no significant role in nucleation, and instead dissolve after extended simulation times, and that nucleation proceeds via aggregation of ion pairs that can be described from a purely classical nucleation theory based framework [9]. Such differences manifest in the experimental range shown in Figure 2, which arises from fitting a speciation model to the linear binding profile from potentiometric titration measurements [10, 53]. The methodological framework developed in this work is primed for extension to tackle this increased complexity of multiple ion aggregation. The fixed topology of many classical force fields again makes MLPs particularly amenable to explore reactivity questions between carbonate, bicarbonate and carbonic acid [18]. Finally, obtaining reliable thermodynamics of the ions in solution relative to the solid-state will necessitate models that can faithfully reproduce the experimental solubility [14], and so obtaining hydration free

energies within our MLP framework will be an important next step [69].

The comparison between DFT and cWFT methods also highlights the importance of explicitly describing the solvent degrees of freedom at the same high level of theory as the main species of interest. For example, implicit solvation models continue to be the workhorse for large scale studies of chemical reactivity in solution [70]. We show that entropic contributions to the ion pairing differ significantly from CCSD(T) to lower levels of theory, while previous work also highlighted the significant challenges in reproducing water properties with DFT [24, 49]. Therefore, the approach developed in this paper serves as a route forward for modeling reactivity and the behaviour of ions in solution, where both the solvent and reactive components can be treated on an equal footing at a high level of theory.

Finally, while still an order of magnitude or so slower than classical force fields, our MLP approach has allowed the accumulation of microseconds worth of cWFT-quality simulations. This has enabled us to obtain uncertainties on the free energies, entropy and enthalpy that are of the same order as those from classical forcefield simulations. This has been made possible by coupling the efficient Symmetrix library (a C++, Kokkos optimized MACE implementation [71, 72]) and the efficiency of OPES. In terms of the cost investment in training the models, the majority of the computational cost actually comes from the periodic MP2 calculations, while the CCSD(T) gas phase calculations are comparatively cheaper.

## CONCLUSIONS

In this paper we have introduced an approach to study ions in solution at the ‘gold-standard’ CCSD(T) level of accuracy. This work generalizes previous  $\Delta$ -machine-learning approaches for liquid water to now handle the increased complexity of solvated ions. We combine this with state of the art enhanced sampling methods to converge both the accuracy of the PES and statistical sampling, while explicitly treating the solvent degrees of freedom. We show such a level of accuracy on the PES is necessary to obtain reliable agreement to experiments on the free energy, enthalpy and entropy, with no other *ab initio* methods capable of simultaneously getting all three within experimental uncertainties. This reliability has also enabled new atomistic understanding into ion pairing as well as the hydration structure around ions, highlighting salient differences with lower levels of theory. Such detailed insights into the solvation structure of individual ions are challenging to obtain experimentally while its reliability can be difficult to ascertain when inferred from empirical force-field simulations.

The approach taken within this work can readily be adopted by other research groups. All the codes used are freely available to academics and we provide the models, steps and code to generate the data for  $\Delta$ -learning. We

expect little modification is required to extend this towards other solution-based processes such as chemical reactions [73] as well as higher concentrations of ions. We also foresee exciting new developments on the horizon on both the electronic structure theory and MLP fronts that will significantly benefit our approach. For example, explicit treatment of long-range electrostatic interactions in the MLPs should allow for more diverse systems, including interfaces and highly charged systems, that are difficult to describe by current purely short-ranged models [74, 75], while ongoing developments in obtaining gradients of the CCSD(T) PES [76] will further facilitate the training of such models for more complex and demanding systems.

Besides being able to derive new insights, the routine development of CCSD(T) models opens a new paradigm towards the development of newer, cost-efficient methods. For example, classical force fields typically require parameterization against experimental data, which are not always readily available and can obscure mechanistic interpretation, whereas the CCSD(T) models developed here provide both quantitative accuracy and direct mechanistic insight. Nevertheless, the next steps towards, for example, nucleation will still pose an arduous computational challenge even for the relative efficiency of the models trained here. The idea of using these models to train cheaper, more efficient MLP architectures in the spirit of knowledge distillation [77] while in principle retaining the CCSD(T) quality is an exciting one for further exploration. Additionally these models will also be useful for benchmarking DFT functionals, where we show that commonly used functionals for aqueous systems, such as revPBE-D3 and revPBE0-D3, fail to achieve quantitative accuracy with experiment for the ion pair association free energy of  $\text{CaCO}_3$ . By bringing CCSD(T)-level accuracy to explicitly solvated systems, this work lays the foundation for predictive simulations of complex chemical processes in solution.

## METHODS

### Machine learning potentials

In this paper we follow two approaches to develop MLPs at various levels of electronic structure theory. The key details are described here, with a more thorough description given in Section 1 of the SI. The ML framework used in this work is based on the MACE architecture [78], which has been shown to be particularly successful in faithfully reproducing the underlying PES with high accuracy [79] and data efficiency.

For all reference methods up to and including MP2 we use standard protocols to fit MLPs to periodic reference data. For CCSD(T) accuracy we correct this ‘lower-level’ cWFT PES using a  $\Delta$ -learning procedure.

**Periodic models:** The models based on revPBE-D3, revPBE0-D3, RPA and MP2 were trained using periodic

reference data labelled with energies and forces. We exploit highly efficient implementations of both RPA [26] and MP2 [28] within the CP2K code [80] which provides access to both energies and gradients for periodic boundary conditions (PBCs).

We use a 2-step process to obtain reliable models as illustrated in the central panel of Figure 1, where first the PES is roughly sampled to generate an initial model that is then systematically improved in a second targeted sampling step. A common initial dataset sampled from previous AIMD simulations [13] containing roughly 300 structures was used to generate initial models for each level of theory. We emphasise that AIMD simulations are not strictly necessary, and indeed sampling configurations from foundation models or classical force field simulations is sufficient to obtain a reliable initial model.

We and others have shown in particular that sampling from a range of (positive and negative) pressures, generates robust models for stable simulations in the isothermal-isobaric ensemble [24, 49]. Therefore, after generating an initial model, it is then refined to ensure that it is quantitatively accurate for the underlying reference level of theory, as well as suitable for NPT simulations, by sampling using the first generation model over a range of pressures, as well as from biased simulations to ensure adequate sampling over the various solvated and ion pairing states. We find that simply one extra round of iterative training, as described, results in models that can then be immediately used in simulations to obtain thermodynamic properties. The total number of configurations in each of the final models was between 700 - 900. All periodic models were trained on energies and forces with 2 message passing layers with 128 channels and a 6 Å radial cutoff.

**$\Delta$ -learning workflow:** To obtain the CCSD(T) level models, we employ a  $\Delta$ -learning strategy that we first introduce in Ref. [49]. We generalise our approach for bulk water to now tackle ions in solution. The general strategy is that a baseline model trained on energies and forces at the MP2 level is corrected to CCSD(T) using clusters of the solvated ion pair cleaved out from bulk simulations at the MP2 level as depicted in the left-most panel of Figure 1. An important consideration when increasing the complexity beyond bulk water is that clusters containing ions will have a significant dipole moment, which grows as the ions get further apart. This is an issue for DFT since it is more susceptible to dielectric breakdown because it tends to underestimate the band gap [81]. On the other hand, cWFT methods like MP2 are not susceptible to this dielectric breakdown since they are based on Hartree-Fock, which has a better treatment of the band gap. This is the reason why MP2 was used as the baseline in this work rather than DFT as in our previous work on liquid water [49]. The CCSD(T)  $\Delta$ -model was trained on the energy differences between MP2 and CCSD(T).

In practice, a similar 2-step procedure as the periodic models was used, where first, clusters are cut from the MP2

dataset to give an initial CCSD(T)-level model. The cluster dataset was then augmented by cutting out clusters from NPT simulations over a range of pressures and solvation states using the initial CCSD(T) model to give the final CCSD(T)  $\Delta$ -model. The clusters were cut such that all waters within a 5.5 Å cutoff of each ion in the ion pair were included (as illustrated in Figure 2 of the SI). All clusters contained an ion pair and were thus neutral. The final  $\Delta$  model contained 1133 configurations in the dataset.

In summary, this simple framework combines many advances in methods across the materials modeling field, namely electronic structure methods, machine learning architectures, implementations and training procedures and enhanced sampling algorithms to develop models that can provide accurate thermodynamic insight at cWFT levels of theory. Additional details on the models, including training errors and validation tests for both the periodic and  $\Delta$  CCSD(T) model are given in Section 1 of the SI. In particular we show that the  $\Delta$ -CCSD(T) approach learning from MP2 can reliably correct the known deficiencies of MP2 for bulk water, where it overstructures the oxygen-oxygen radial distribution function [30].

## Coupled Cluster Theory

For the (cluster-based) dataset used to train the  $\Delta$ -MLP, we calculated MP2 with local approximations [82, 83] (LMP2) and CCSD(T) with the local natural orbital approximation (LNO) [84, 85]. These calculations were both performed in MRCC [86], with the LMP2 numbers coming naturally from the LNO-CCSD(T) calculation. We used the default “normal” LNO thresholds – recently validated for the properties of water in Ref. [49] – and use density-fitting (with the def2-QZVPP-RI-JK auxiliary basis set) to speed up the HF calculations. We included the sub-valence correlation of the 3s and 3p electrons on the Ca atom with the corresponding cc-pwCVXZ [87, 88] basis set, where X represents the cardinal number. We use the aug-cc-pVXZ basis set on the O and cc-pVXZ basis set on the H and C atoms, while the cc-pwCVXZ basis set was used for the Ca atoms. For all other atoms, we used the cc-pVXZ family of (valence) basis sets, in particular using the diffuse aug-cc-pVXZ basis sets on the O atom. For the auxiliary basis sets required for the LNO-CCSD(T) calculations, we used those generated in Ref. [89] Ref. [90] for each atom. However, as none were available for Ca, we used the automatic auxiliary basis functions code of Stoychev *et al.* [91, 92] to generate these basis functions. We performed complete basis set (CBS) extrapolations for the double (DZ) and triple-zeta (TZ) basis sets, using parameters taken from Neese and Valeev [93].

## Periodic DFT + MP2

All reference calculations were done on a unit cell of length  $\sim 14$  Å containing 126 waters and one ion pair. revPBE-D3 calculations were performed with FHI-AIMs [94], using the tight family of basis sets and Grimme's D3 (zero-damping variant) [55]. All periodic calculations were performed at the  $\Gamma$ -point. revPBE0-D3, RPA and MP2 calculations were performed with the CP2K/Quickstep [80] code. The electronic density was partitioned into core and valence electrons, with core electrons described with the norm-conserving Goedecker, Teter and Hutter (GTH) pseudopotentials [95]. For revPBE0-D3, hydrogen and oxygen atoms were described with the TZV2P family of basis sets, while we used the ccGRB family for carbon and hydrogen. revPBE0-D3 calculations used the auxiliary density matrix methods (ADMM) approximation [96] to improve the efficiency. For RPA and MP2 we used the cc-TZ basis set for oxygen and hydrogen, with the ccGRB basis set for carbon and calcium. PBE was used as a starting point for the RPA correlation energy calculations. The resolution-of-identity (RI) technique was used for these methods [97]. We used triple-zeta (TZ) quality correlation-consistent basis sets for H and O (taken from CP2Ks RI\_cc\_TZ\_set) and correlation-consistent basis sets designed by Ye and Berkelbach [98] for carbon and calcium. Auxiliary basis sets for the RI integral operations were generated using the automatic auxiliary basis of Stoychev et al. [91, 92] for calcium and carbon, with the defaults (from CP2K) used for H and O. For consistency with previously developed models [23] a planewave cutoff of 1200 Ry was used in the CP2K calculations (although in practice the forces are converged after around 400 Ry).

## Molecular Dynamics

All simulations were performed using the Large-scale Atomic Molecular Massively Parallel Simulator (LAMMPS) [99] code combined with PLUMED [100], coupled with the Symmetrix library [71, 79], using the symmetrix/mace pair style in tandem with the hybrid/overlay pairstyle to sum the MP2 baseline and  $\Delta$ -MLPs.

## Free energy calculations

All MLP-based simulations to obtain the free energies were performed in a simulation box of length  $\sim 18$  Å with 197 waters and 1 CaCO<sub>3</sub> ion pair. For each level of theory, the equilibrium density was first obtained for a given temperature from simulations in the NPT ensemble using the CSVr thermostat [101] with a temperature relaxation time of 0.1 ps and a 1.0 fs timestep using a deuterium masses for hydrogen atoms. These trajectories were then

used to generate initial configurations for the OPES simulations to obtain the free energy profiles from which the association free energies were computed [51]. The efficient convergence behavior of OPES was used to enable multiple replicas to obtain sufficient statistics to robustly estimate the free energy of ion pairing. For each level of theory, simulations were performed at 5 temperatures (300, 310, 320, 330, 340 K). At each temperature 6 independent replicas were initialized from randomized velocities from the Maxwell-Boltzmann distribution for the given temperature, and run for between 20 - 30 ns each. The bias update frequency was 500 steps, and the barrier for maximum free energy exploration 30 kJ/mol following Ref. [18], with the Ca - CO<sub>3</sub> separation being explicitly biased. The Ca-O<sub>H<sub>2</sub>O</sub> coordination number was computed on the OPES trajectory via a smooth switching function:

$$S(r) = \frac{1 - (r - r_0)^6}{1 - (r - r_0)^{12}}. \quad (1)$$

with  $r_0$  set to 1.9 Å to overlap with the first peak in the Ca-O RDF. After  $\sim 1 - 3$  ns the bias during the simulation had stabilised, enabling reversible exploration of the free energy landscape.

The unbiased probability distribution ( $P(d, n)$ ) was reconstructed from the OPES simulations by reweighting the OPES trajectory using the time-dependent bias potential  $V_{\text{bias}}$ , as a function of both collective variables, the Ca-CO<sub>3</sub> separation ( $d(\mathbf{r})$ ) and the Ca-O<sub>H<sub>2</sub>O</sub> coordination number ( $n(\mathbf{r})$ ):

$$P(d, n) = \frac{\langle \delta(d - d(\mathbf{r})) \delta(n - n(\mathbf{r})) e^{\beta V_{\text{bias}}(\mathbf{r})} \rangle_V}{\langle e^{\beta V_{\text{bias}}(\mathbf{r})} \rangle_V} \quad (2)$$

where  $\langle \cdot \rangle_V$  corresponds to the ensemble average taken over the biased simulation. The final free energy surface is then given by:

$$F(d, n) = -k_B T \ln P(d, n) \quad (3)$$

To obtain the binding free energies, the Ca-O coordination number first was integrated out from the 2D free energy to give the 1D PMF  $\phi(\mathbf{r})$ . The tail of the PMF was then aligned with the analytic solution of two point charges  $q_i$  and  $q_j$  interacting via a screened dielectric potential with dielectric constant  $\epsilon_r$ :

$$\Delta G = \frac{1}{4\pi\epsilon_0} \frac{q_i q_j}{\epsilon_r r} - k_B T \ln(4\pi r^2). \quad (4)$$

with the final standard ion pairing free energy  $\Delta G_{\text{IP}}^\ominus$  then given by integrating the aligned PMF ( $\phi'(r)$ ) up to the edge of the bound state  $R_c$ :

$$\Delta G_{\text{IP}}^\ominus = -RT \ln \left[ 4\pi c^\ominus \int_0^{R_c} r^2 \exp\left(-\frac{\phi'(r)}{k_B T}\right) dr \right]. \quad (5)$$

We used the experimental value of the dielectric constant  $\epsilon_r$  (78), and show in Figure 5 of the SI the sensitivity of our

results to this choice. The extent of finite size effects on the binding free energies and enthalpy/entropy calculations reported in Figure 10 in the SI was tested using a classical force field [14] on a  $\sim 50 \text{ \AA}^3$  box containing 5319 waters and one ion pair.

### DATA AVAILABILITY

All data required to reproduce the findings of this study will be made available upon publication of this study.

### CODE AVAILABILITY

All simulations were performed with publicly available simulation software (ACEsuit, LAMMPS, Symmetrix and PLUMED).

### ACKNOWLEDGMENTS

N.O.N acknowledges financial support from the Gates Cambridge Trust and is grateful for an International Exchange Grant funded by the Royal Society. The Flatiron Institute is a division of the Simons Foundation. W.C.W. acknowledges support from the EPSRC (Grant EP/V062654/1). A.M. acknowledges support from the European Union under the “n-AQUA” European Research Council project (Grant No. 101071937). J.D.G and B.I.A thank the Australian Research Council for funding under grant FL180100087, as well as the Pawsey Supercomputing Centre and National Computational Infrastructure for computing resources. C.S. acknowledges financial support from the Royal Society, grant number RGS/R2/242614 and the Isaac Newton Trust, award number G122390. We are grateful for computational support and resources from the UK national high-performance computing service, Advanced Research Computing High End Resource (ARCHER2). Access for ARCHER2 were obtained via the UK Car-Parrinello consortium, funded by EPSRC grant reference EP/P022561/1. We also acknowledge the EuroHPC Joint Undertaking for awarding this project access to the EuroHPC supercomputer LEONARDO, hosted by CINECA (Italy) and the LEONARDO consortium through an EuroHPC Regular Access call. This work was also performed using resources provided by the Cambridge Service for Data Driven Discovery (CSD3) operated by the University of Cambridge Research Computing Service ([www.csd3.cam.ac.uk](http://www.csd3.cam.ac.uk)), provided by Dell EMC and Intel using Tier-2 funding from the Engineering and Physical Sciences Research Council (capital grant EP/T022159/1), and DiRAC funding from the Science and Technology Facilities Council ([www.dirac.ac.uk](http://www.dirac.ac.uk))

\* [cs2121@cam.ac.uk](mailto:cs2121@cam.ac.uk)

† [am452@cam.ac.uk](mailto:am452@cam.ac.uk)

‡ [J.Gale@curtin.edu.au](mailto:J.Gale@curtin.edu.au)

- [1] H. Lu, Y.-C. Huang, J. Hunger, D. Gebauer, H. Cölfen, and M. Bonn, Role of water in  $\text{CaCO}_3$  biomineralization, *J. Am. Chem. Soc.* **143**, 1758 (2021).
- [2] L. Cao, D. Li, E. Hu, J. Xu, T. Deng, L. Ma, Y. Wang, X.-Q. Yang, and C. Wang, Solvation structure design for aqueous Zn metal batteries, *J. Am. Chem. Soc.* **142**, 21404 (2020).
- [3] S. H. C. Noonan, C. Birrell, R. Fisher, and K. E. Fabricius, Progressive changes in coral reef communities with increasing ocean acidification, *Commun. Biol.* **8**, 1518 (2025).
- [4] L. Huang, A. Babaahmadi, K. M. Rosso, J. J. De Yoreo, and X. Zhang, Bridging mechanisms and materials to scale  $\text{CO}_2$  mineralization for carbon storage, *Nat. Rev. Mater.* , **1** (2026).
- [5] C. Hepburn, E. Adlen, J. Beddington, E. A. Carter, S. Fuss, N. Mac Dowell, J. C. Minx, P. Smith, and C. K. Williams, The technological and economic prospects for  $\text{CO}_2$  utilization and removal, *Nature* **575**, 87 (2019).
- [6] P. J. M. Smeets, K. R. Cho, R. G. E. Kempen, N. A. J. M. Sommerdijk, and J. J. De Yoreo, Calcium carbonate nucleation driven by ion binding in a biomimetic matrix revealed by in situ electron microscopy, *Nat. Mater.* **14**, 394 (2015).
- [7] P. Raiteri and J. D. Gale, Water is the key to nonclassical nucleation of amorphous calcium carbonate, *J. Am. Chem. Soc.* **132**, 17623 (2010).
- [8] D. Gebauer, A. Völkel, and H. Cölfen, Stable prenucleation calcium carbonate clusters, *Science* **322**, 1819 (2008).
- [9] P. J. M. Smeets, A. R. Finney, W. J. E. M. Habraken, F. Nudelman, H. Friedrich, J. Laven, J. J. De Yoreo, P. M. Rodger, and N. A. J. M. Sommerdijk, A classical view on nonclassical nucleation, *Proc. Natl. Acad. Sci. U. S. A.* **114**, E7882 (2017).
- [10] D. Gebauer and H. Cölfen, Prenucleation clusters and nonclassical nucleation, *Nano Today* **6**, 564 (2011).
- [11] R. Demichelis, P. Raiteri, J. D. Gale, D. Quigley, and D. Gebauer, Stable prenucleation mineral clusters are liquid-like ionic polymers, *Nat. Commun.* **2**, 590 (2011).
- [12] D. Gebauer, M. Kellermeier, J. D. Gale, L. Bergström, and H. Cölfen, Pre-nucleation clusters as solute precursors in crystallisation, *Chemical Society Reviews* **43**, 2348 (2014).
- [13] P. Raiteri, A. Schuitemaker, and J. D. Gale, Ion pairing and multiple ion binding in calcium carbonate solutions based on a polarizable AMOEBA force field and *ab initio* molecular dynamics, *J. Phys. Chem. B* **124**, 3568 (2020).
- [14] B. Armstrong, A. Silvestri, R. Demichelis, P. Raiteri, and J. D. Gale, Solubility-consistent force field simulations for aqueous metal carbonate systems using graphical processing units, *Philos. Trans. R. Soc., A* **381**, 20220250 (2023).
- [15] F. Neese, M. Atanasov, G. Bistoni, D. Maganas, and S. Ye, Chemistry and quantum mechanics in 2019: Give us insight and numbers, *J. Am. Chem. Soc.* **141**, 2814 (2019).
- [16] D. P. McDonogh, J. D. Gale, P. Raiteri, and D. Gebauer, Redefined ion association constants have consequences for calcium phosphate nucleation and biomineralization, *Nat. Commun.* **15**, 3359 (2024).
- [17] J. Aufort, P. Raiteri, and J. D. Gale, Computational insights into  $\text{Mg}^{2+}$  dehydration in the presence of carbonate,

- ACS Earth Space Chem. **6**, 733 (2022).
- [18] P. M. Piaggi, J. D. Gale, and P. Raiteri, Ab initio machine-learning simulation of calcium carbonate from aqueous solutions to the solid state, *Proc. Natl. Acad. Sci. U. S. A.* **122**, e2415663122 (2025).
- [19] K. R. Bryenton, A. A. Adeleke, S. G. Dale, and E. R. Johnson, Delocalization error: The greatest outstanding challenge in density-functional theory, *Wiley Interdiscip. Rev.:Comput. Mol. Sci.* **13**, e1631 (2023).
- [20] F. Jensen, Describing anions by density functional theory: Fractional electron affinity, *J. Chem. Theory Comput.* **6**, 2726 (2010).
- [21] A. Otero-de-la-Roza and E. R. Johnson, Analysis of density-functional errors for noncovalent interactions between charged molecules, *J. Phys. Chem. A* **124**, 353 (2020).
- [22] O. A. Vydrov, G. E. Scuseria, and J. P. Perdew, Tests of functionals for systems with fractional electron number, *J. Chem. Phys.* **126**, 154109 (2007).
- [23] N. O'Neill, B. X. Shi, K. Fong, A. Michaelides, and C. Schran, To pair or not to pair? Machine-learned explicitly-correlated electronic structure for NaCl in water, *J. Phys. Chem. Lett.* **15**, 6081 (2024).
- [24] P. Montero de Hijes, C. Dellago, R. Jinnouchi, and G. Kresse, Density isobar of water and melting temperature of ice: Assessing common density functionals, *J. Chem. Phys.* **161**, 131102 (2024).
- [25] T. T. Duignan, G. K. Schenter, J. L. Fulton, T. Huthwelker, M. Balasubramanian, M. Galib, M. D. Baer, J. Wilhelm, J. Hutter, M. D. Ben, X. S. Zhao, and C. J. Mundy, Quantifying the hydration structure of sodium and potassium ions: Taking additional steps on Jacob's Ladder, *Phys. Chem. Chem. Phys.* **22**, 10641 (2020).
- [26] M. Del Ben, O. Schütt, T. Wentz, P. Messmer, J. Hutter, and J. VandeVondele, Enabling simulation at the fifth rung of DFT: Large scale RPA calculations with excellent time to solution, *Comput. Phys. Commun.* **187**, 120 (2015).
- [27] M. Del Ben, J. Hutter, and J. VandeVondele, Electron correlation in the condensed phase from a resolution of identity approach based on the Gaussian and plane waves scheme, *J. Chem. Theory Comput.* **9**, 2654 (2013).
- [28] M. Del Ben, J. Hutter, and J. VandeVondele, Forces and stress in second order Møller-Plesset perturbation theory for condensed phase systems within the resolution-of-identity Gaussian and plane waves approach, *J. Chem. Phys.* **143**, 102803 (2015).
- [29] S. Y. Willow, X. C. Zeng, S. S. Xantheas, K. S. Kim, and S. Hirata, Why is MP2-water "cooler" and "denser" than DFT-water?, *J. Phys. Chem. Lett.* **7**, 680 (2016).
- [30] M. Del Ben, M. Schönherr, J. Hutter, and J. VandeVondele, Bulk liquid water at ambient temperature and pressure from MP2 theory, *J. Phys. Chem. Lett.* **4**, 3753 (2013).
- [31] A. Zen, J. G. Brandenburg, J. Klimeš, A. Tkatchenko, D. Alfè, and A. Michaelides, Fast and accurate quantum Monte Carlo for molecular crystals, *Proceedings of the National Academy of Sciences* **115**, 1724 (2018).
- [32] A. Karton, E. Rabinovich, J. M. L. Martin, and B. Ruscic, W4 theory for computational thermochemistry: In pursuit of confident sub-kJ/mol predictions, *J. Chem. Phys.* **125**, 144108 (2006).
- [33] B. X. Shi, A. S. Rosen, T. Schäfer, A. Grüneis, V. Kapil, A. Zen, and A. Michaelides, An accurate and efficient framework for modelling the surface chemistry of ionic materials, *Nat. Chem.* **17**, 1688 (2025).
- [34] B. X. Shi, A. Zen, V. Kapil, P. R. Nagy, A. Grüneis, and A. Michaelides, Many-body methods for surface chemistry come of age: Achieving consensus with experiments, *J. Am. Chem. Soc.* **145**, 25372 (2023).
- [35] T. Schäfer, F. Libisch, G. Kresse, and A. Grüneis, Local embedding of coupled cluster theory into the random phase approximation using plane waves, *J. Chem. Phys.* **154**, 011101 (2021).
- [36] J. P. Carbone, A. Irmiler, A. Gallo, T. Schäfer, W. Z. V. Benschoten, J. J. Shepherd, and A. Grüneis, CO adsorption on Pt(111) studied by periodic coupled cluster theory, *Faraday Discuss.* **254**, 586 (2024).
- [37] J. Yang, W. Hu, D. Usvyat, D. Matthews, M. Schütz, and G. K.-L. Chan, Ab initio determination of the crystalline benzene lattice energy to sub-kilojoule/mole accuracy, *Science* **345**, 640 (2014).
- [38] H.-Z. Ye and T. C. Berkelbach, Adsorption and vibrational spectroscopy of CO on the surface of MgO from periodic local coupled-cluster theory, *Faraday Discuss.* **254**, 628 (2024).
- [39] H.-Z. Ye and T. C. Berkelbach, Periodic local coupled-cluster theory for insulators and metals, *J. Chem. Theory Comput.* **20**, 8948 (2024).
- [40] K. Yu, C. M. Krauter, J. M. Dieterich, and E. A. Carter, Density and Potential Functional Embedding: Theory and Practice, in *Fragmentation* (John Wiley & Sons, Ltd, 2017) Chap. 2, pp. 81–117.
- [41] J. M. P. Martirez and E. A. Carter, Solvent dynamics are critical to understanding carbon dioxide dissolution and hydration in water, *J. Am. Chem. Soc.* **145**, 12561 (2023).
- [42] J.-N. Boyn and E. A. Carter, Characterizing the mechanisms of Ca and Mg carbonate ion-pair formation with multi-level molecular dynamics/quantum mechanics simulations, *J. Phys. Chem. B* **127**, 10824 (2023).
- [43] H. Agnew, R. Savoj, R. Rashmi, B. Savala, and F. Paesani, Molecular insights into the influence of ions on the water structure. II. Halide ions in solution, *J. Phys. Chem. B* **129**, 6584 (2025).
- [44] R. Savoj, H. Agnew, R. Zhou, and F. Paesani, Molecular insights into the influence of ions on the water structure. I. Alkali metal ions in solution, *J. Phys. Chem. B* **128**, 1953 (2024).
- [45] S. Saha and F. Paesani, Hydration free energies of alkali and halide ions from data-driven many-body potentials, *ChemRxiv* **2026**, 10.26434/chemrxiv.15000607/v1.
- [46] C. Qu, Q. Yu, P. L. Houston, R. Conte, A. Nandi, and J. M. Bowman, Interfacing q-AQUA with a polarizable force field: The best of both worlds, *J. Chem. Theory Comput.* **19**, 3446 (2023).
- [47] J. Daru, H. Forbert, J. Behler, and D. Marx, Coupled cluster molecular dynamics of condensed phase systems enabled by machine learning potentials: Liquid water benchmark, *Phys. Rev. Lett.* **129**, 226001 (2022).
- [48] M. S. Chen, J. Lee, H.-Z. Ye, T. C. Berkelbach, D. R. Reichman, and T. E. Markland, Data-efficient machine learning potentials from transfer learning of periodic correlated electronic structure methods: Liquid water at AFQMC, CCSD, and CCSD(T) accuracy, *J. Chem. Theory Comput.* **19**, 4510 (2023).
- [49] N. O'Neill, B. X. Shi, W. J. Baldwin, W. C. Witt, G. Csányi, J. D. Gale, A. Michaelides, and C. Schran, Towards routine condensed phase simulations with delta-learned coupled cluster accuracy: Application to liquid wa-

- ter, *J. Chem. Theory Comput.* **21**, 11710 (2025).
- [50] R. Ramakrishnan, P. O. Dral, M. Rupp, and O. A. von Lilienfeld, Big data meets quantum chemistry approximations: The  $\Delta$ -machine learning approach, *J. Chem. Theory Comput.* **11**, 2087 (2015).
- [51] M. Invernizzi and M. Parrinello, Rethinking metadynamics: From bias potentials to probability distributions, *J. Phys. Chem. Lett.* **11**, 2731 (2020).
- [52] M. Kellermeier, P. Raiteri, J. K. Berg, A. Kempter, J. D. Gale, and D. Gebauer, Entropy drives calcium carbonate ion association, *ChemPhysChem* **17**, 3535 (2016).
- [53] L. N. Plummer and E. Busenberg, The solubilities of calcite, aragonite and vaterite in  $\text{CO}_2$ - $\text{H}_2\text{O}$  solutions between 0 and 90°C, and an evaluation of the aqueous model for the system  $\text{CaCO}_3$ - $\text{CO}_2$ - $\text{H}_2\text{O}$ , *Geochim. Cosmochim. Acta* **46**, 1011 (1982).
- [54] Y. Zhang and W. Yang, Comment on “Generalized Gradient Approximation Made Simple”, *Phys. Rev. Lett.* **80**, 890 (1998).
- [55] S. Grimme, J. Antony, S. Ehrlich, and H. Krieg, A consistent and accurate *ab initio* parametrization of density functional dispersion correction (DFT-D) for the 94 elements H-Pu, *J. Chem. Phys.* **132**, 154104 (2010).
- [56] C. Adamo and V. Barone, Toward reliable density functional methods without adjustable parameters: The PBE0 model, *J. Chem. Phys.* **110**, 6158 (1999).
- [57] L. Goerigk and S. Grimme, A thorough benchmark of density functional methods for general main group thermochemistry, kinetics, and noncovalent interactions, *Phys. Chem. Chem. Phys.* **13**, 6670 (2011).
- [58] Hitoshi. Ohtaki and Tamas. Radnai, Structure and dynamics of hydrated ions, *Chem. Rev.* **93**, 1157 (1993).
- [59] N. A. Hewish, G. W. Neilson, and J. E. Enderby, Environment of  $\text{Ca}^{2+}$  ions in aqueous solvent, *Nature* **297**, 138 (1982).
- [60] F. Jalilehvand, D. Spångberg, P. Lindqvist-Reis, K. Hermansson, I. Persson, and M. Sandström, Hydration of the calcium ion. An EXAFS, large-angle X-ray scattering, and molecular dynamics simulation study, *J. Am. Chem. Soc.* **123**, 431 (2001).
- [61] T. Megyes, T. Grósz, T. Radnai, I. Bakó, and G. Pálinkás, Solvation of calcium ion in polar solvents: An X-ray diffraction and *ab initio* study, *J. Phys. Chem. A* **108**, 7261 (2004).
- [62] B. S. González, J. Hernández-Rojas, and D. J. Wales, Global minima and energetics of  $\text{Li}^+(\text{H}_2\text{O})_n$  and  $\text{Ca}^{2+}(\text{H}_2\text{O})_n$  clusters for  $n \leq 20$ , *Chemical Physics Letters* **412**, 23 (2005).
- [63] T. Ikeda, M. Boero, and K. Terakura, Hydration properties of magnesium and calcium ions from constrained first principles molecular dynamics, *J. Chem. Phys.* **127**, 074503 (2007).
- [64] J.-N. Boyn and E. A. Carter, Probing pH-dependent dehydration dynamics of Mg and Ca cations in aqueous solutions with multi-level quantum mechanics/molecular dynamics simulations, *J. Am. Chem. Soc.* **145**, 20462 (2023).
- [65] D. Jiao, C. King, A. Grossfield, T. A. Darden, and P. Ren, Simulation of  $\text{Ca}^{2+}$  and  $\text{Mg}^{2+}$  solvation using polarizable atomic multipole potential, *J. Phys. Chem. B* **110**, 18553 (2006).
- [66] M. M. Naor, K. V. Nostrand, and C. Dellago, Car-Parrinello molecular dynamics simulation of the calcium ion in liquid water, *Chem. Phys. Lett.* **369**, 159 (2003).
- [67] A. F. Wallace, L. O. Hedges, A. Fernandez-Martinez, P. Raiteri, J. D. Gale, G. A. Waychunas, S. Whitelam, J. F. Banfield, and J. J. De Yoreo, Microscopic evidence for liquid-liquid separation in supersaturated  $\text{CaCO}_3$  solutions, *Science* **341**, 885 (2013).
- [68] Z. Zou, W. J. E. M. Habraken, L. Bertinetti, Y. Politi, A. Gal, S. Weiner, L. Addadi, and P. Fratzl, On the phase diagram of calcium carbonate solutions, *Adv. Mater. Interfaces* **4**, 1600076 (2017).
- [69] J. Harry Moore, D. J. Cole, and G. Csányi, Computing solvation free energies of small molecules with experimental accuracy, *J. Am. Chem. Soc.* **148**, 4928 (2026).
- [70] A. V. Marenich, C. J. Cramer, and D. G. Truhlar, Universal solvation model based on solute electron density and on a continuum model of the solvent defined by the bulk dielectric constant and atomic surface tensions, *J. Phys. Chem. B* **113**, 6378 (2009).
- [71] W. C. Witt, Symmetrix, available at: <https://github.com/wcwitt/symmetrix> (2026).
- [72] D. P. Kovács, J. H. Moore, N. J. Browning, I. Batatia, J. T. Horton, Y. Pu, V. Kapil, W. C. Witt, I.-B. Magdău, D. J. Cole, and G. Csányi, MACE-OFF: Short-range transferable machine learning force fields for organic molecules, *J. Am. Chem. Soc.* **147**, 17598 (2025).
- [73] H. Zhang, V. Juraskova, and F. Duarte, Modelling chemical processes in explicit solvents with machine learning potentials, *Nat. Commun.* **15**, 6114 (2024).
- [74] S. Yue, M. C. Muniz, M. F. Calegari Andrade, L. Zhang, R. Car, and A. Z. Panagiotopoulos, When do short-range atomistic machine-learning models fall short?, *J. Chem. Phys.* **154**, 034111 (2021).
- [75] S. P. Niblett, M. Galib, and D. T. Limmer, Learning intermolecular forces at liquid-vapor interfaces, *J. Chem. Phys.* **155**, 164101 (2021).
- [76] X. Zhang and G. K.-L. Chan, Differentiable quantum chemistry with PySCF for molecules and materials at the mean-field level and beyond, *J. Chem. Phys.* **157**, 204801 (2022).
- [77] J. L. A. Gardner, D. F. T. du Toit, C. B. Mahmoud, Z. F. Beaulieu, V. Juraskova, L.-B. Paşca, L. A. M. Rosset, F. Duarte, F. Martelli, C. J. Pickard, and V. L. Deringer, Distillation of atomistic foundation models across architectures and chemical domains (2025), [arXiv:2506.10956 \[physics\]](https://arxiv.org/abs/2506.10956).
- [78] I. Batatia, D. P. Kovacs, G. Simm, C. Ortner, and G. Csanyi, MACE: Higher order equivariant message passing neural networks for fast and accurate force fields, *Advances in Neural Information Processing Systems* **35**, 11423 (2022).
- [79] D. P. Kovács, I. Batatia, E. S. Arany, and G. Csányi, Evaluation of the MACE force field architecture: From medicinal chemistry to materials science, *J. Chem. Phys.* **159**, 044118 (2023).
- [80] T. D. Kühne, M. Iannuzzi, M. Del Ben, V. V. Rybkin, P. Seewald, F. Stein, T. Laino, R. Z. Khaliullin, O. Schütt, F. Schiffmann, D. Golze, J. Wilhelm, S. Chulkov, M. H. Bani-Hashemian, V. Weber, U. Borštnik, M. Taillefumier, A. S. Jakobovits, A. Lazzaro, H. Pabst, T. Müller, R. Schade, M. Guidon, S. Andermatt, N. Holmberg, G. K. Schenter, A. Hehn, A. Bussy, F. Belleflamme, G. Tabacchi, A. GlöB, M. Lass, I. Bethune, C. J. Mundy, C. Plessl, M. Watkins, J. VandeVondele, M. Krack, and J. Hutter, CP2K: An electronic structure and molecular dynamics software package - Quickstep: Efficient and accurate elec-

- tronic structure calculations, *J. Chem. Phys.* **152**, 194103 (2020).
- [81] J. P. Perdew, Density functional theory and the band gap problem, *Int. J. Quantum Chem.* **28**, 497 (1985).
- [82] P. R. Nagy, G. Samu, and M. Kállay, An integral-direct linear-scaling second-order Møller–Plesset approach, *J. Chem. Theory Comput.* **12**, 4897 (2016).
- [83] P. B. Szabó, J. Csóka, M. Kállay, and P. R. Nagy, Linear-scaling open-shell MP2 approach: Algorithm, benchmarks, and large-scale applications, *J. Chem. Theory Comput.* **17**, 2886 (2021).
- [84] P. R. Nagy, G. Samu, and M. Kállay, Optimization of the linear-scaling local natural orbital CCSD(T) method: Improved algorithm and benchmark applications, *J. Chem. Theory Comput.* **14**, 4193 (2018).
- [85] L. Gyevi-Nagy, M. Kállay, and P. R. Nagy, Integral-direct and parallel implementation of the CCSD(T) method: Algorithmic developments and large-scale applications, *J. Chem. Theory Comput.* **16**, 366 (2020).
- [86] M. Kállay, P. R. Nagy, D. Mester, Z. Rolik, G. Samu, J. Csontos, J. Csóka, P. B. Szabó, L. Gyevi-Nagy, B. Hégyel, I. Ladjánszki, L. Szegedy, B. Ladóczki, K. Petrov, M. Farkas, P. D. Mezei, and Á. Ganyecz, The MRCC program system: Accurate quantum chemistry from water to proteins, *J. Chem. Phys.* **152**, 074107 (2020).
- [87] K. A. Peterson and T. H. Dunning, Jr., Accurate correlation consistent basis sets for molecular core–valence correlation effects: The second row atoms Al–Ar, and the first row atoms B–Ne revisited, *J. Chem. Phys.* **117**, 10548 (2002).
- [88] N. B. Balabanov and K. A. Peterson, Systematically convergent basis sets for transition metals. I. All-electron correlation consistent basis sets for the 3d elements Sc–Zn, *J. Chem. Phys.* **123**, 064107 (2005).
- [89] F. Weigend, M. Häser, H. Patzelt, and R. Ahlrichs, RI-MP2: Optimized auxiliary basis sets and demonstration of efficiency, *Chem. Phys. Lett.* **294**, 143 (1998).
- [90] A. Hellweg, C. Hättig, S. Höfener, and W. Klopper, Optimized accurate auxiliary basis sets for RI-MP2 and RI-CC2 calculations for the atoms Rb to Rn, *Theor. Chem. Acc.* **117**, 587 (2007).
- [91] G. L. Stoychev, A. A. Auer, and F. Neese, Automatic generation of auxiliary basis sets, *J. Chem. Theory Comput.* **13**, 554 (2017).
- [92] S. Lehtola, Straightforward and accurate automatic auxiliary basis set generation for molecular calculations with atomic orbital basis sets, *J. Chem. Theory Comput.* **17**, 6886 (2021).
- [93] F. Neese and E. F. Valeev, Revisiting the atomic natural orbital approach for basis sets: Robust systematic basis sets for explicitly correlated and conventional correlated *ab initio* methods?, *J. Chem. Theory Comput.* **7**, 33 (2011).
- [94] V. Blum, R. Gehrke, F. Hanke, P. Havu, V. Havu, X. Ren, K. Reuter, and M. Scheffler, *Ab Initio* molecular simulations with numeric atom-centered orbitals, *Comput. Phys. Commun.* **180**, 2175 (2009).
- [95] S. Goedecker, M. Teter, and J. Hutter, Separable dual-space Gaussian pseudopotentials, *Phys. Rev. B* **54**, 1703 (1996).
- [96] M. Guidon, J. Hutter, and J. VandeVondele, Auxiliary density matrix methods for Hartree-Fock exchange calculations, *J. Chem. Theory Comput.* **6**, 2348 (2010).
- [97] A. Bussy, O. Schütt, and J. Hutter, Sparse tensor based nuclear gradients for periodic Hartree–Fock and low-scaling correlated wave function methods in the CP2K software package: A massively parallel and GPU accelerated implementation, *J. Chem. Phys.* **158**, 164109 (2023).
- [98] H.-Z. Ye and T. C. Berkelbach, Correlation-consistent Gaussian basis sets for solids made simple, *J. Chem. Theory Comput.* **18**, 1595 (2022).
- [99] A. P. Thompson, H. M. Aktulga, R. Berger, D. S. Bolintineanu, W. M. Brown, P. S. Crozier, P. J. in 't Veld, A. Kohlmeyer, S. G. Moore, T. D. Nguyen, R. Shan, M. J. Stevens, J. Tranchida, C. Trott, and S. J. Plimpton, LAMMPS - A flexible simulation tool for particle-based materials modeling at the atomic, meso, and continuum scales, *Comput. Phys. Commun.* **271**, 108171 (2022).
- [100] M. Bonomi, G. Bussi, C. Camilloni, G. A. Tribello, P. Banáš, A. Barducci, M. Bernetti, P. G. Bolhuis, S. Bottaro, D. Branduardi, R. Capelli, P. Carloni, M. Ceriotti, A. Cesari, H. Chen, W. Chen, F. Colizzi, S. De, M. De La Pierre, D. Donadio, V. Drobot, B. Ensing, A. L. Ferguson, M. Filizola, J. S. Fraser, H. Fu, P. Gasparotto, F. L. Gervasio, F. Giberti, A. Gil-Ley, T. Giorgino, G. T. Heller, G. M. Hocky, M. Iannuzzi, M. Invernizzi, K. E. Jelfs, A. Jussupow, E. Kirilin, A. Laio, V. Limongelli, K. Lindorff-Larsen, T. Löhr, F. Marinelli, L. Martin-Samos, M. Masetti, R. Meyer, A. Michaelides, C. Molteni, T. Morishita, M. Nava, C. Paissoni, E. Papaleo, M. Parrinello, J. Pfaendtner, P. Piaggi, G. Piccini, A. Pietropaolo, F. Pietrucci, S. Pipolo, D. Provasi, D. Quigley, P. Raiteri, S. Raniolo, J. Rydzewski, M. Salvalaglio, G. C. Sosso, V. Spiwok, J. Šponer, D. W. H. Swenson, P. Tiwary, O. Valsson, M. Vendruscolo, G. A. Voth, A. White, and The PLUMED consortium, Promoting transparency and reproducibility in enhanced molecular simulations, *Nat. Methods* **16**, 670 (2019).
- [101] G. Bussi, D. Donadio, and M. Parrinello, Canonical sampling through velocity rescaling, *J. Chem. Phys.* **126**, 014101 (2007).

# Supporting Information for: “From Accurate Quantum Chemistry to Converged Thermodynamics for Ion Pairing in Solution ”

(Dated: March 10, 2026)

## CONTENTS

1. Models	2
A. Periodic models	2
1. Validation of periodic models	3
B. CCSD(T) model	3
1. Validation of $\Delta$ -CCSD(T) model	4
2. Electronic Structure	5
A. Coupled Cluster Theory and MP2 for cluster calculations	5
B. Periodic DFT + MP2	6
3. Bader charge analysis	6
4. Simulations	7
A. Ion pairing free energy	8
1. Convergence of OPES simulations	11
2. Computing enthalpy and entropy	13
3. Finite size effects and error analysis	16
B. Ion coordination free energies	17
5. Comparison to previous cWFT literature	18
6. Comparison to classical force-field	19
References	19

## 1. MODELS

All of the MLPs in this work are based on the MACE framework [1]. Two approaches for obtaining MLPs were used depending on the reference method. For the DFT, RPA and MP2 - based models, routine protocols based on fitting to *periodic reference data* were used, as described in 1 A below. To obtain CCSD(T)-level models, a  $\Delta$ -*learning approach* first introduced in Ref.[2] was used, whereby a periodic MP2 model was ‘corrected’ up to CCSD(T)-level of theory using a second  $\Delta$ -model trained on the difference between MP2 and CCSD(T) energies only. This is described in greater detail in Section 1 B below.

### A. Periodic models

All models were trained over multiple generations, with the aim of faithfully reproducing the potential energy surface (PES) of the underlying level of theory. An initial dataset of  $\text{CaCO}_3$ , sampled from previous *ab initio* simulations from Ref. [3] was used to generate an initial ‘Generation-1’ model at various levels of theory (revPBE-D3, revPBE0-D3, RPA, MP2). As well as targeting the standard energy and force RMSEs with respect to a validation set, we found that directly benchmarking the models against desired thermodynamic properties was important. Therefore we also ‘self-consistently’ converged the models for the density and ion pairing free energy. In a second generation to ensure a robust dataset the following conditions were sampled using the Generation 1 models at each level of theory:

- Configurations sampled from equilibrium molecular dynamics (MD) trajectories of 126-water boxes with one  $\text{Ca-CO}_3$  ion pair generated at a range of pressures (specifically -1500, -500, -300, 1, 2, 500, 1000, 4000, 8000 bar). Such density and pressure fluctuations have been shown to be important to obtain reliable densities [2, 4].
- Configurations obtained from well-tempered metadynamics to ensure complete sampling of both the ion pair separation and the coordination environments.

All periodic models comprised two message passing layers, with 128 channels and a radial cutoff of 6 Å. There was a 5 % train/test split and training was run for 300 epochs, where the energy weight of the loss function was increased to 1000 for the last 50 epochs.

### 1. Validation of periodic models

Training errors on the energies and forces are given in Table 1. The final density prediction

Model	Train-Energy [meV/atom]	Validation-Energy [meV/atom]	Train-Forces [meV/Å]	Validation-Forces [meV/Å]
revPBE-D3	0.3	0.3	25.1	26.1
revPBE0-D3	0.6	0.6	26.9	27.1
RPA	0.3	0.2	28.6	29.2
MP2	0.3	0.3	25.6	26.3

**TABLE 1:** Training and validation errors for the final periodic models trained in this work.

of all the models for bulk water is shown in Figure 1. Since we are in the end targeting a single Ca/CO<sub>3</sub> ion pair in solution, this will have minimal effect on the density and so comparing to bulk water has more reliable experimental values as well as from previous literature.

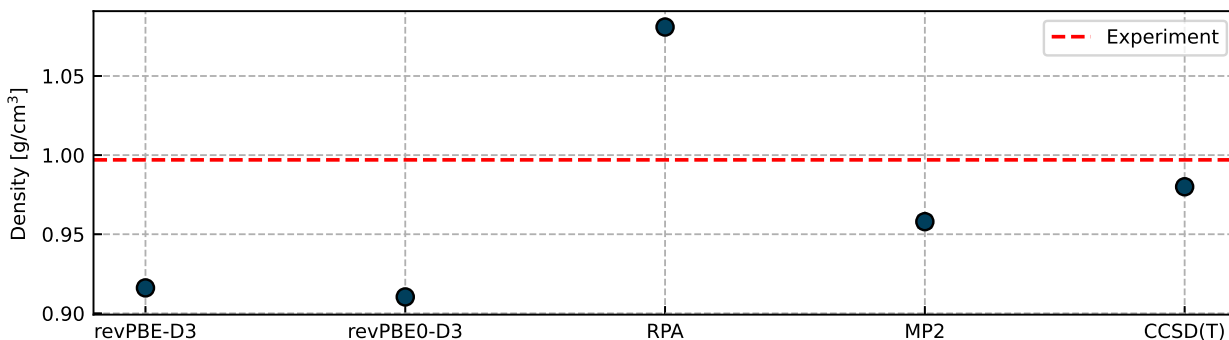


**FIG. 1: Validation of periodic models against bulk water density:** Density of bulk water for the levels of theory studied in this work compared to experiment at 298 K.

### B. CCSD(T) model

The protocol to develop the CCSD(T) model is based on the framework we introduced in Ref. [2]. The dataset for the  $\Delta$  model was generated by cleaving clusters from periodic MP2 configurations, obtained from the pressure scan and metadynamics simulations described in the above section for generating the periodic dataset. All waters within a  $\sim 5.5$  Å radius of each ion pair were included, where such a cluster size was chosen such that the ions were sufficiently

solvated, while also allowing for affordable computational cost for the CCSD(T) calculations. Figure 2 shows a typical cluster. The  $\Delta$ -model was then trained on the energy differences between

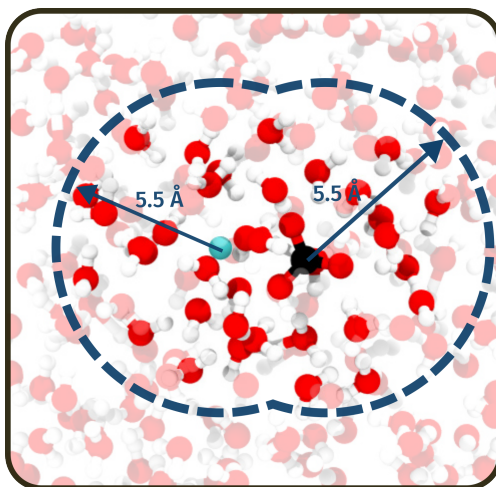


**FIG. 2:** Example cluster cut from periodic configuration. All waters within 5.5 Å of each of the Ca and CO<sub>3</sub> are included (ensuring that the full molecule is included in the cluster i.e. no broken bonds).

MP2 and CCSD(T) for this dataset. We used a smaller model architecture here, comprising 128 channels with 2 message passing layers and a 5 Å radial cutoff, which we showed in Ref. [2] improves the efficiency (where there is otherwise a penalty of summing 2 MLPs) without any sacrifice on the accuracy or reliability. The final  $\Delta$ -CCSD(T) model had energy errors of 0.1 meV/atom on both training and validation sets and the final dataset comprised 1133 structures.

### 1. Validation of $\Delta$ -CCSD(T) model

Extensive validation tests on our  $\Delta$ -learning protocol using a DFT baseline are included in Ref. [2]. To show that our model can reliably correct the difference between MP2 and CCSD(T), in this Section, we validate it against a system with now well-established references for both MP2 and CCSD(T) – liquid water. In Figure 3, we compare the RDFs predicted by the MP2 baseline model – which is known to overstructure [5] liquid water – with the prediction of the  $\Delta$ -CCSD(T) model. We also include the CCSD(T) model developed in Ref. [2] for comparison. The  $\Delta$ -CCSD(T) model corrects the general overstructuring of the RDFs from MP2, especially the first peak of the O-O RDF and the hydrogen bonding peak of the O-H RDF. Furthermore, it is in excellent agreement with the CCSD(T) model from Ref. [2].

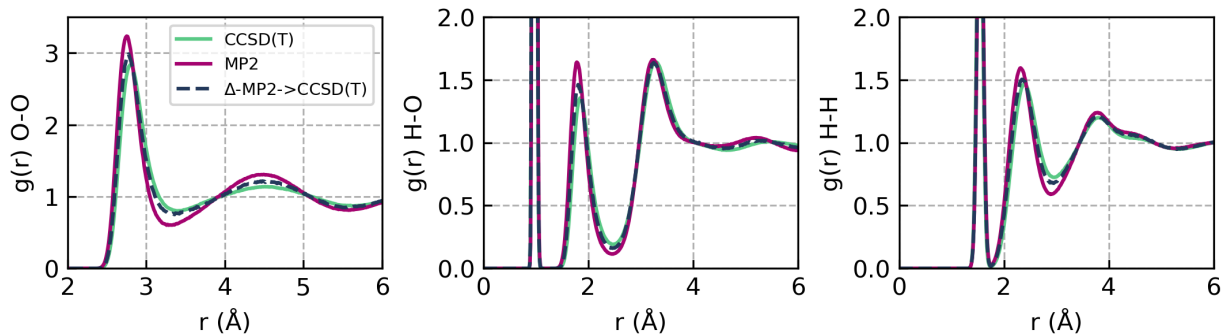


**FIG. 3:** Comparison of  $\Delta$ -CCSD(T) model for bulk water structure, with periodic MP2 baseline (pink) and CCSD(T) model trained in Ref. [2] (green). Note all simulations here have been performed with classical nuclei at 298 K.

## 2. ELECTRONIC STRUCTURE

Here the details of both the periodic and gas-phase calculations used for training the MLPs are described. For completeness, some of the information given in the Methods Section of the main manuscript is repeated.

### A. Coupled Cluster Theory and MP2 for cluster calculations

For the (cluster-based) dataset used to train the  $\Delta$ -MLP, we calculated MP2 with local approximations [6, 7] (LMP2) and CCSD(T) with the local natural orbital approximation (LNO) [8, 9], respectively. These calculations were both performed in MRCC [10], with the LMP2 numbers coming naturally from the LNO-CCSD(T) calculation. We used the default “normal” LNO thresholds – recently validated for the properties of water [2] – and use density-fitting (with the def2-QZVPP-RI-JK auxiliary basis set) to speed up the HF calculations. We included the sub-valence correlation of the 3s and 3p electrons on the Ca atom with the corresponding cc-pwCVXZ [11, 12] basis set, where  $X$  represents the cardinal number. We use the aug-cc-pVXZ basis set on the O and cc-pVXZ basis set on the H and C atoms, while the cc-pwCVXZ basis set was use for the Ca atoms. For all other atoms, we used the cc-pVXZ family (valence) basis sets, in particular using the diffuse aug-cc-pVXZ basis sets on the O atom. For the auxiliary basis sets required for the LNO-CCSD(T) calculations, we used those generated in Ref. [13] Ref. [14] for each atom. However, as none were available for Ca, we used the automatic auxiliary basis functions code of Stoychev *et al.* [15, 16] to generate these basis functions. We performed

complete basis set (CBS) extrapolations for the double (DZ) and triple-zeta (TZ) basis sets, using parameters taken from Neese and Valeev [17].

## B. Periodic DFT + MP2

All reference calculations were done on a unit cell of length  $\sim 14$  Å containing 126 waters and one ion pair. revPBE-D3 calculations were performed with FHI-AIMs [18], using the tight family of basis sets and the (in-built) Grimme's D3 [19]. All periodic unit cell calculations were performed using the  $\Gamma$ -point. revPBE0-D3, RPA and MP2 calculations were performed with the CP2K/Quickstep [20] code. The electronic density was partitioned into core and valence electrons, with core electrons described with the norm-conserving Goedecker, Teter and Hutter (GTH) pseudopotentials [21]. For revPBE0-D3, hydrogen and oxygen atoms were described with the TZV2P family of basis sets, while we used the ccGRB family for carbon and hydrogen. revPBE0-D3 calculations used the auxiliary density matrix methods (ADMM) approximation [22] to improve the efficiency. For RPA and MP2 we used the cc-TZ basis set for oxygen and hydrogen, with the ccGRB basis set for carbon and calcium. PBE was used as a starting point for the RPA correlation energy calculations. The resolution-of-identity (RI) techniques was used for these methods [23] We used triple-zeta (TZ) quality correlation consistent basis sets for H and O (taken from CP2K's RI\_cc\_TZ set) and correlation consistent basis sets designed by Ye and Berkelbach [24] for carbon and calcium. Auxiliary basis sets for the RI integral operations were generated using the automatic auxiliary basis of Stoychev et al. [15, 16] for calcium and carbon, with the defaults (from CP2K) used for H and O. For consistency with previously developed models [5] a planewave cutoff of 1200 Ry was used (although in practice the forces are converged after around 400 Ry).

## 3. BADER CHARGE ANALYSIS

One of the well-documented shortcomings of DFT is its inability (to varying extents) to localise charge [25, 26]. This is in general evident in the 1-dimensional potential of mean force, where going from GGA (revPBE-D3) to hybrid (revPBE0-D3) to MP2 and CCSD(T) results in increasingly stable contact ion pair states. To explore this further this we used the Bader charge partitioning scheme to assign partial charges on the solvated ions predicted by the studied levels of theory in this work. Figure 4 shows the Bader charges on the  $\text{Ca}^{2+}$  and  $\text{CO}_3^{2-}$  ions. For

each ion, 100 snapshots were sampled from a trajectory containing the individual ion in a box of 63 waters. The electronic density was then computed on these snapshots, and the Bader charge obtained using the Bader code from the Henkelman group [27]. For both the  $\text{Ca}^{2+}$  and  $\text{CO}_3^{2-}$ , there is a trend of  $\text{revPBE-D3} < \text{revPBE0-D3} < \text{RPA} < \text{MP2}$  for the extent of charge localisation. This is consistent with the expected degree of delocalisation error with DFT [25]. There is also a clear correlation between the extent of charge delocalisation and the depth of the contact ion pair minima in the 1-D PMFs in Figure 3 in the main text.

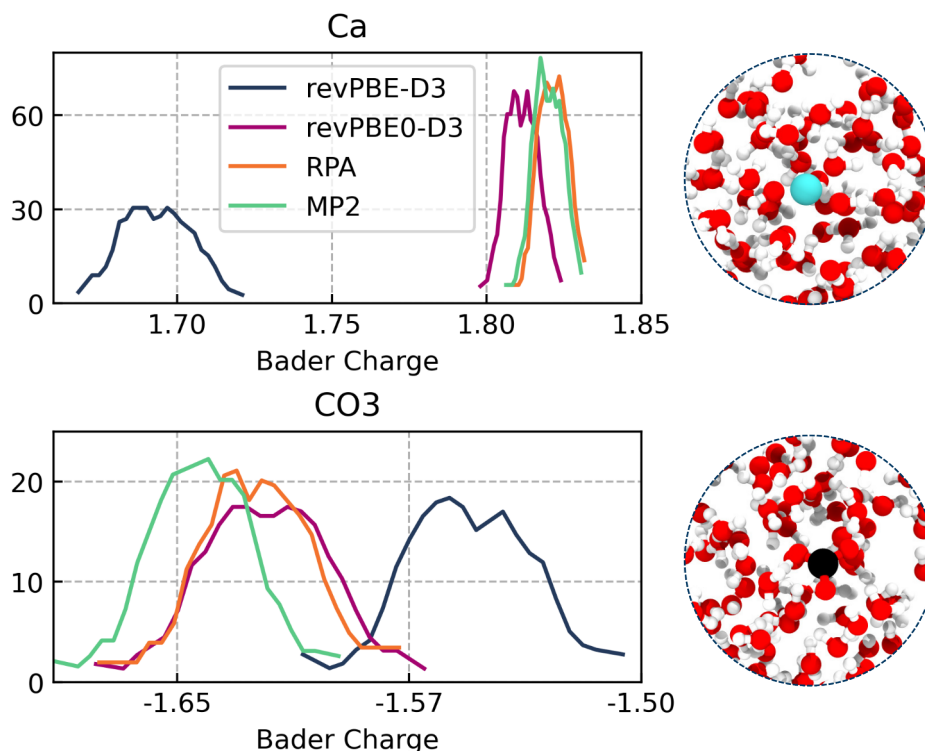


**FIG. 4: Bader charge distribution by functional** Bader charges on solvated  $\text{Ca}^{2+}$  and  $\text{CO}_3^{2-}$  ions computed at increasing levels of electronic structure theory. The snapshots show the box, of one  $\text{Ca}^{2+}$  ( $\text{CO}_3^{2-}$ ) ion surrounded by 63 waters.

#### 4. SIMULATIONS

For clarity, all MLP results shown in the SI are reported without finite size effects, to enable future comparison with our setup. The final results presented in the main paper have been corrected for finite size effects, which are discussed in detail below. All simulations were performed using the Large-scale Atomic Molecular Massively Parallel Simulator (LAMMPS) [28] code, combined with PLUMED [29] and coupled with the Symmetrix library [30, 31], using the `symmetrix/mace`

pair style in tandem with the hybrid/overlay pairstyle to sum the MP2 baseline and  $\Delta$ -MLPs. All classical forcefield simulations used the parameters developed in Ref. [32] for  $\text{CaCO}_3$  in water.

### A. Ion pairing free energy

The calculation of ion pairing free energies has received substantial previous attention, and so here we summarise the main key steps and considerations, as well as showing convergence tests to reassure the reliability of our final results. For a thorough description and discussion, the reader is referred to the supplementary information of Ref. [33]. The free energy profiles were obtained from on-the-fly probability enhanced (OPES) [34] simulations, where the Ca- $\text{CO}_3$  ion pair separation was used as the collective variable to be biased. It has been previously shown that sampling the orthogonal Ca-water coordination number is important to obtain reliable estimates of the free energy. Therefore the Ca- $\text{O}_{\text{H}_2\text{O}}$  coordination number was computed on-the-fly on the biased OPES trajectory via a smooth switching function  $S(r)$ :

$$S(r) = \frac{1 - (r - r_0)^6}{1 - (r - r_0)^{12}}. \quad (1)$$

with  $r_0$  set to 1.9 Å to overlap with the first peak in the Ca-O RDF.

The unbiased probability distribution ( $P(d, n)$ ) was reconstructed from the OPES simulations by reweighting the OPES trajectory using the time-dependant bias potential  $V_{\text{bias}}$ , as a function of both collective variables, the Ca- $\text{CO}_3$  separation ( $d(\mathbf{r})$ ) and the Ca- $\text{O}_{\text{H}_2\text{O}}$  coordination number ( $n(\mathbf{r})$ ):

$$P(d, n) = \frac{\langle \delta(d - d(\mathbf{r})) \delta(n - n(\mathbf{r})) e^{\beta V_{\text{bias}}(\mathbf{r})} \rangle_V}{\langle e^{\beta V_{\text{bias}}(\mathbf{r})} \rangle_V} \quad (2)$$

where  $\langle \cdot \rangle_V$  corresponds to the ensemble average taken over the biased simulation. The final free energy surface is then given by:

$$F(d, n) = -k_B T \ln P(d, n) \quad (3)$$

We note that it was important to first recover the 2D free energy, since there are some orthogonal steps to the Ca- $\text{CO}_3$  separation. To ensure the correct asymptotic behaviour, the tail of the PMF is aligned with the analytical solution for the pairing free energy of two point charges  $q_i, q_j$  interacting via a screened electrostatic potential:

$$\Delta G = \frac{1}{4\pi\epsilon_0} \frac{q_i q_j}{\epsilon_r r} - k_B T \ln(4\pi r^2). \quad (4)$$

where  $\epsilon_r$  is the dielectric constant of the medium. The standard ion pairing free energy  $\Delta G_{\text{IP}}^{\ominus}$  can then be obtained by integrating the aligned PMF ( $\phi'(r)$ ) up to  $R_c$ :

$$\Delta G_{\text{IP}}^{\ominus} = -RT \ln \left[ 4\pi c^{\ominus} \int_0^{R_c} r^2 \exp \left( -\frac{\phi'(r)}{k_B T} \right) dr \right]. \quad (5)$$

Here  $c^{\ominus}$  is a concentration unit conversion from atoms/ $\text{\AA}^3$  to mol/ $\text{dm}^3$  required to correctly relate the simulated association free energy to that obtained from experiment. The choice of  $R_c$  has been shown to only weakly effect the resulting association constant (provided that the free energy profile is correctly aligned to the tail of the analytic solution) [33], and so here we use  $R_c$  as 7  $\text{\AA}$ .

Furthermore, since the MACE potential does not contain charge information, we make an approximation and use the experimental dielectric constant (78) to align the PMF to the analytic solution. Figure 5 shows the dependence of the association free energy (for the CCSD(T) model)

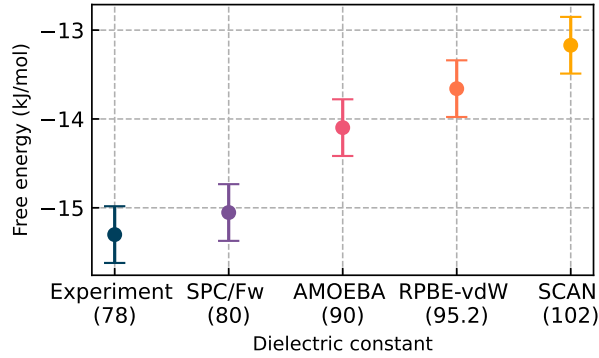


**FIG. 5: Effect of dielectric constant on association free energy:** Comparison of ion pairing free energy for the CCSD(T) model at 300 K using different values for the dielectric constant (values for the dielectric constant given in brackets beneath the model name). RPBE-vdW value from Ref. [35] and SCAN from Ref. [36].

to the choice of dielectric constant, spanning experiment, non-polarisable (SPC/Fw) [37] and polarisable (AMOEBA) [38] force field, as well as the value for some DFT functionals that have been published in the literature. The dielectric constant for SCAN [36] and RPBE-vdW [35] are both greater than experiment, which subsequently shifts the free energy systematically by up to 2 kJ/mol. Nevertheless, given previous benchmarking on other properties of liquid water for CCSD(T) [2] including density and diffusion, we expect that the CCSD(T) values of the dielectric constant should be in close agreement with experiment, justifying our choice. However, ongoing

developments in the direction of including explicit electrostatics in MLPs, we anticipate should remove the requirement to make such a choice, since charge information will be readily available.

### 1. Convergence of OPES simulations

To obtain statistically converged estimates for all models, six independent replicas were performed at each temperature, each with a total simulation length of 20–30 ns. To ensure statistical convergence of the final free energy, in Figure 6 we show the free energy of each replica at each temperature as a function of cumulated simulation time. After approximately  $\sim 3$  ns, the OPES

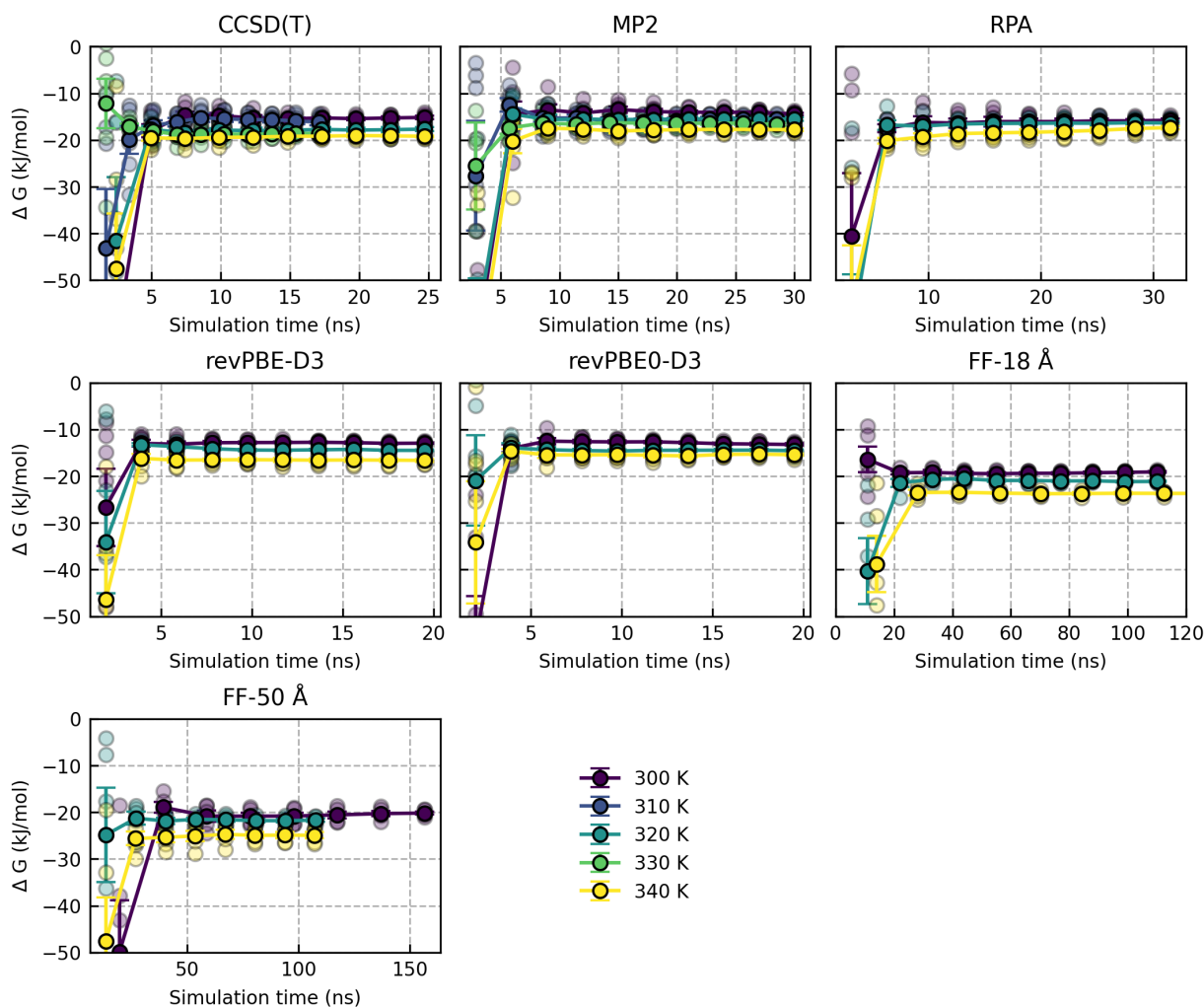


**FIG. 6: OPES convergence:** Convergence of the association free energy computed from integration of the OPES PMF as a function of cumulative simulation time for temperatures from 300-340 K for all the models in this work. The transparent circles show the individual replicas at each temperature, while the translucent circles show the average and standard errors across the replicas as a function of cumulative simulation time.

bias potential had stabilised, after which the simulations reversibly sampled the free-energy surface. This highlights a key advantage of OPES over other enhanced sampling methods, especially

when used with MLPs where computational cost is still a concern: once the bias has stabilised, the majority of the simulation time can be devoted to sampling the flattened free-energy landscape [39].

## 2. Computing enthalpy and entropy

Enthalpy  $\Delta H$  and entropy  $\Delta S$  contributions to the ion pairing free energy were computed assuming the standard thermodynamic relation:

$$\Delta G = \Delta H - T\Delta S \quad (6)$$

A weighted linear regression was performed to account for the uncertainty in the free energy values at each temperature. Figure 7 compares the temperature dependence of  $\Delta G$  and the associated linear fit for all of the models developed in this work, as well as classical forcefield results used for validation and computing finite size effects (see next Section).

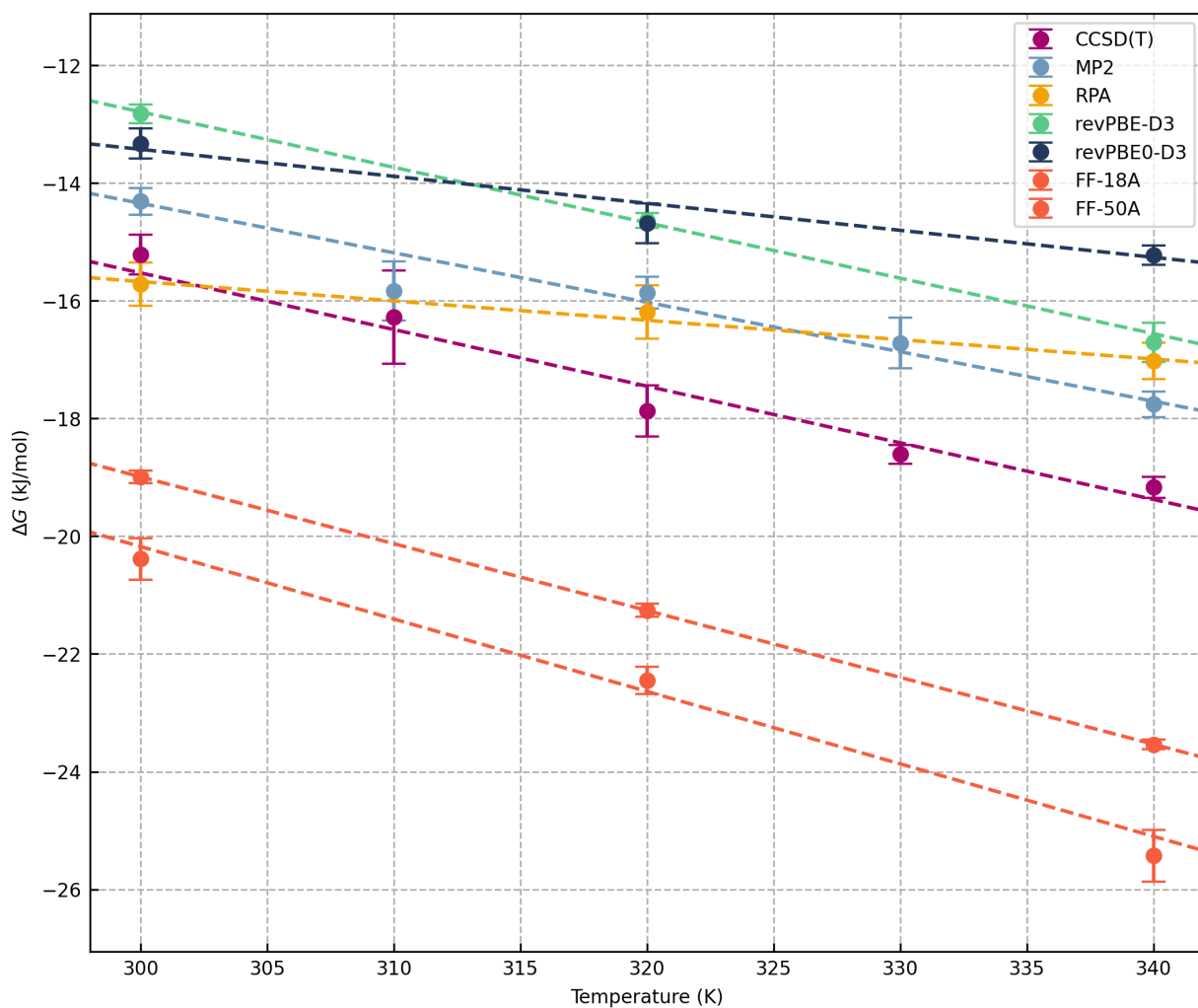


**FIG. 7:  $\Delta G$  vs Temperature** Comparison of  $\Delta G$  versus temperature from OPES simulations for all of the models developed in this work. Classical force field results are also shown for the 18 Å and 50 Å boxes used to compute finite-size effects.

In Figures 8 and 9, the 1D PMFs at each temperature for each method are also shown (from which  $\Delta G$  were computed), where there is a general trend of increasing CIP stability with increasing temperature for all methods (as has been previously observed for classical forcefield models [32]).

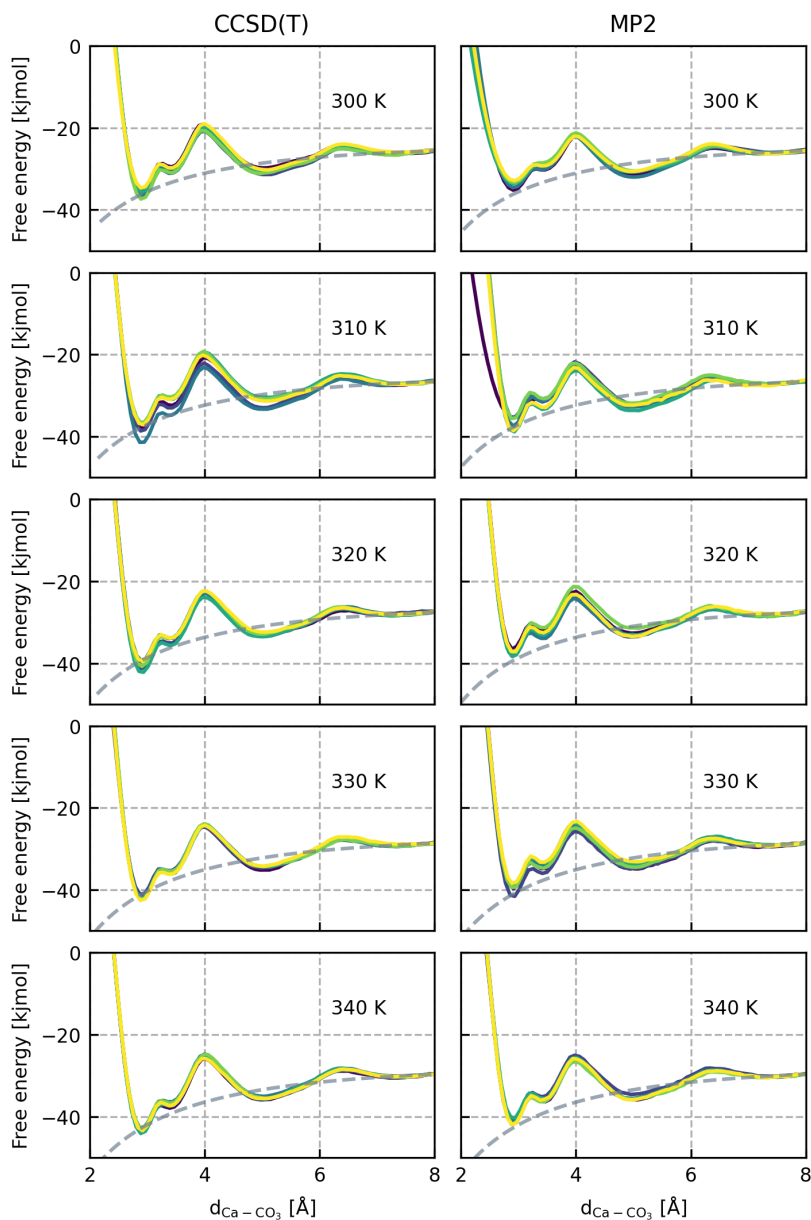


**FIG. 8: 1D PMFs – cWFT:** Free energy as a function of Ca–CO<sub>3</sub> separation for CCSD(T) and MP2 models at 300,310,320,330 and 340 K. Each plot shows 6 profiles obtained from independent OPES simulations, as well as the analytical solution to which the tail is aligned.

Finally to validate the OPES simulation set-up, in Table 2 we compare the results obtained from previous well-tempered metadynamics simulations with the non-polarisable classical force-

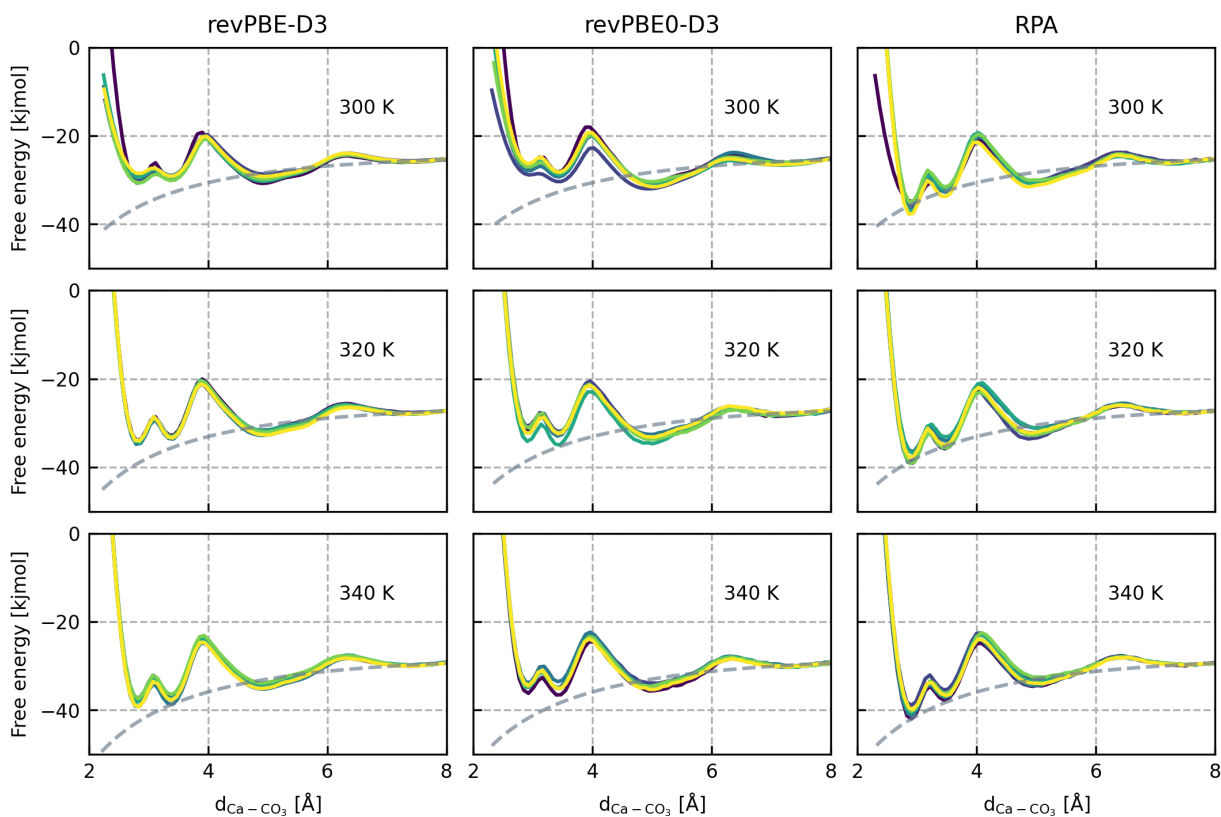


**FIG. 9: 1D PMFs – DFT:** Convergence of the association free energy computed from integration of the OPES PMF as a function of cumulative simulation time for temperatures from 300-340 K for all the models in this work. The transparent circles show the individual replicas at each temperature, while the translucent circles show the average and standard errors across the replicas as a function of cumulative simulation time.

field from Ref. [32] with the OPES setup in this work using the same forcefield parameters.

**TABLE 2:** Comparison of previous FF from well-tempered metadynamics and OPES from this work

Property	This Work	Literature
$\Delta G$ [kJ/mol]	$+20.2 \pm 0.6$	-19.5
$\Delta S$ [J/mol K]	$-114 \pm 22$	$+124 \pm 10$
$\Delta H$ [kJ/mol]	$14.3 \pm 7$	$17.4 \pm 3$

### 3. Finite size effects and error analysis

Despite the significant efficiency boost afforded by MACE over *ab initio* methods, resolving the association free energy still requires substantial simulation effort. While it is standard for classical force fields to resolve the PMF in a 50 Å simulation box, ensuring the tail of the PMF can be aligned at the Bjerrum length, this would be impractical for the MACE models developed in this work. Therefore to quantify the finite size effects arising from the 18 Å box size used in the MLP simulations, we used the most recently developed classical force field parameterised for CaCO<sub>3</sub> in water [32] to compare the results between the 18 Å and 50 Å boxes. This further allowed us to benchmark our OPES setup against the more established well-tempered metadynamics which has been widely used to study this system.

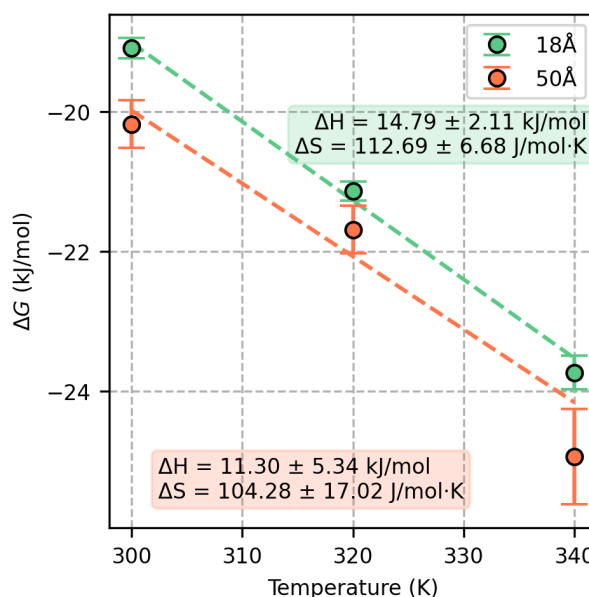


**FIG. 10: Finite size effects:** Comparison of enthalpy and entropy computed from OPES simulations in simulation boxes of length 18 Å and 50 Å with a Ca/CO<sub>3</sub> ion pair and 197 and 5319 waters respectively. Standard errors are obtained from 6 independent simulations at each temperature.

Figure 10 compares the association free energy computed from 10 independent replicas each for both a 18 Å and 50 Å system as a function of temperature. Both setups each contained a single CaCO<sub>3</sub> ion pair and 197 and 5319 waters respectively, and were first equilibrated in the NPT ensemble at each temperature. The finite size effect is roughly constant with temperature and has the effect of increasing the strength of the association energy by roughly 1.12 kJ/mol. Table 3 summarises the corrections. All of the results shown in the main text have been corrected

	18 Å	50 Å	Finite-size effect
$\Delta G_{300K}$ [kJ/mol]	$-19.1 \pm 0.6$	$-20.2 \pm 0.6$	$-1.1 \pm 0.6$
$\Delta H$ [kJ/mol]	$14.8 \pm 2$	$14.3 \pm 7$	$-0.5 \pm 7$
$\Delta S$ [kJ/mol K]	$112.7 \pm 7$	$113.6 \pm 22$	$0.9 \pm 23$

**TABLE 3: Finite size effects:** Comparison of enthalpy, entropy computed from OPES simulations in simulation boxes of length 18 Å and 50 Å with a Ca/CO<sub>3</sub> ion pair and 197 and 5319 waters respectively. Standard errors are obtained from 6 independent simulations at each temperature.

for this finite size effect, and the MLP and classical FF errors have been summed in quadrature.

### B. Ion coordination free energies

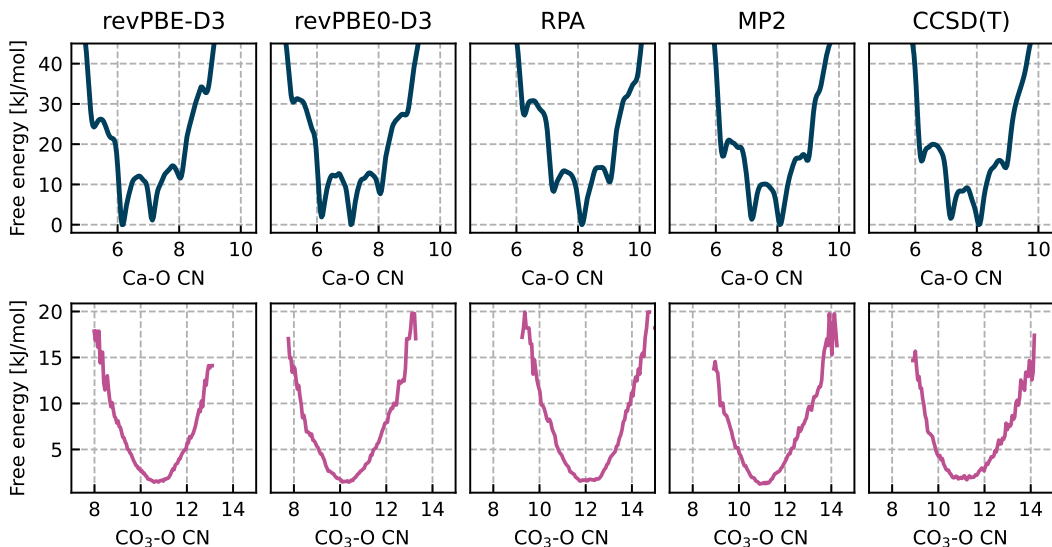


**FIG. 11:** Free energy of Ca<sup>2+</sup> and CO<sub>3</sub><sup>2-</sup> ions in water as a function of water coordination number for all of the levels of theory studied in this work. The lowest point of the curves is aligned to zero.

Figure 11 shows the free energy as a function of water coordination number for the Ca and CO<sub>3</sub> ions. The Ca profile has many free energy minima. Going to increasing levels of theory shifts the profiles towards higher coordinations, with RPA, MP2 and CCSD(T) all giving 8 waters as the lowest free energy, while revPBE-D3, revPBE0-D3 and r<sup>2</sup>SCAN giving 6 and 7 as almost degenerate and the lowest in free energy. The CO<sub>3</sub> profiles are much broader, with fewer discrete coordination states. Here there is a shift towards lower coordination with water

with increasing levels of theory. Comparison of our results with polarizable force field models [32] shows good agreement, with an average calcium (carbonate)-water coordination number of 7.2 (10.7), compared to 7.7 (11.0) predicted by MP2 and CCSD(T).

## 5. COMPARISON TO PREVIOUS CWFT LITERATURE

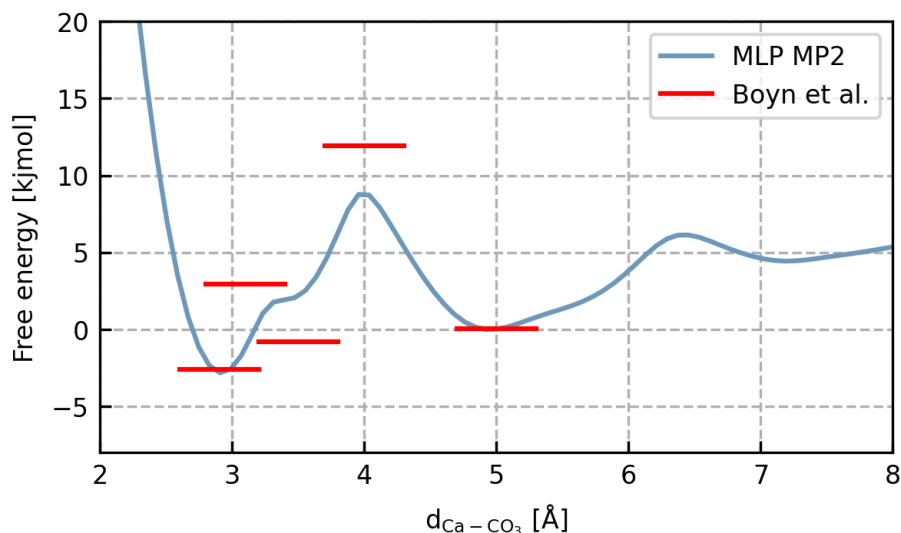


**FIG. 12:** Comparison of MP2 free energy profile obtained from this work at 300 K (blue curve) compared to the corrected features of the DFT PMF to MP2 from Ref. [40] (red lines). The PMF and features are aligned such that the SShIP is at 0.

As described in the main text, previous studies have explored Ca—CO<sub>3</sub> ion pairing in water using quantum embedding approaches at MP2 level [40]. Such an approach only corrects selected features of the PMF, and so in Figure 12, we compare the full MP2 PMF computed in this work with the MP2 features from Boyn *et al.*. The relative stabilities of the bidentate and solvent shared ion pair (SShIP) are in excellent quantitative agreement. Interestingly, the barrier height between CIP and SShIP is significantly larger for the quantum embedding approach compared to our models, suggesting that including entropic effects by explicitly sampling the full CCSD(T) PES is an important consideration to obtain reliable transition state barriers. Differences in our approaches may contribute to the discrepancies in the features of the PMF, where the quantum embedding approach relies on 1) Limited sampling of the DFT level PES from *ab initio* blue moon ensemble simulations, 2) only sampling a single CV (Ca—CO<sub>3</sub> separation), neglecting the orthogonal Ca—O<sub>H<sub>2</sub>O</sub> coordination number and 3) using a small simulation box ( $\sim 12 \text{ \AA}^3$ ).

## 6. COMPARISON TO CLASSICAL FORCE-FIELD

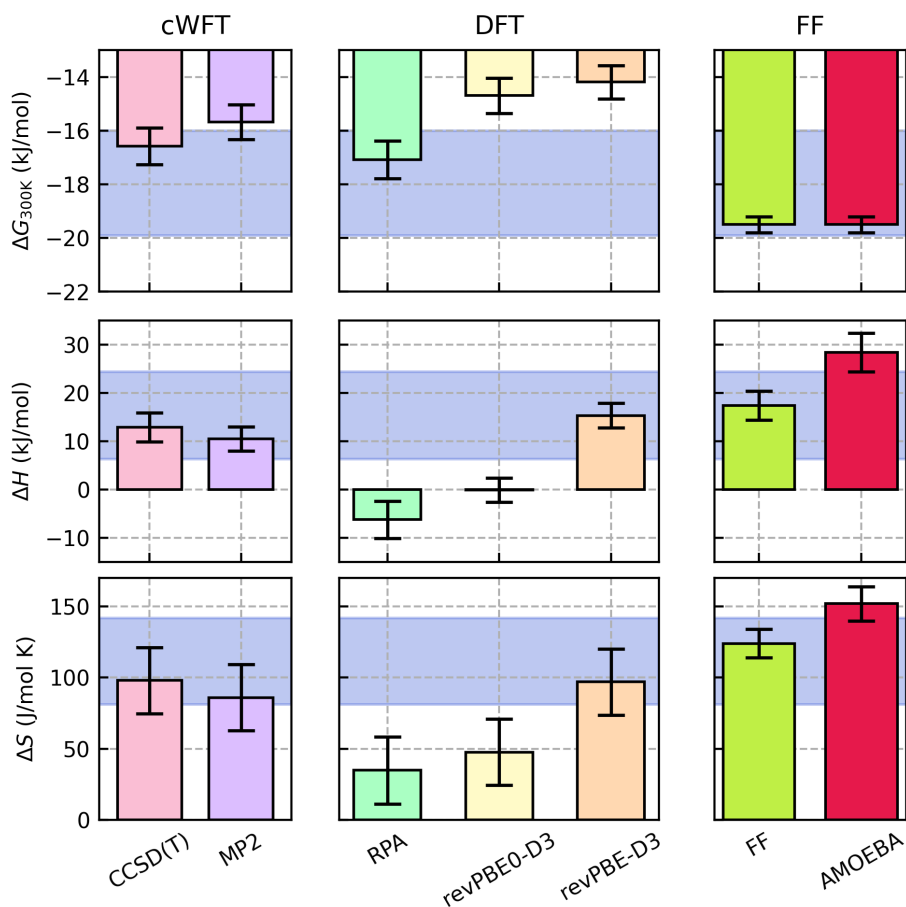


**FIG. 13:** Comparison of cWFT predictions of  $\Delta G$ ,  $\Delta H$  and  $\Delta S$  with classical force field parameterisation from Ref. [32].

Finally, in Figure 13 we compare the enthalpy and entropy predictions of CCSD(T), MP2 and DFT to the predictions of the classical force-field results from Ref. [32], as well as previous results from the AMOEBA polarisable forcefield [3].

[1] I. Batatia, D. P. Kovacs, G. Simm, C. Ortner, and G. Csanyi, MACE: Higher order equivariant message passing neural networks for fast and accurate force fields, *Advances in Neural Information Processing Systems* **35**, 11423 (2022).

[2] N. O'Neill, B. X. Shi, W. J. Baldwin, W. C. Witt, G. Csányi, J. D. Gale, A. Michaelides, and

- C. Schran, Towards routine condensed phase simulations with delta-learned coupled cluster accuracy: Application to liquid water, *J. Chem. Theory Comput.* **21**, 11710 (2025).
- [3] P. Raiteri, A. Schuitemaker, and J. D. Gale, Ion pairing and multiple ion binding in calcium carbonate solutions based on a polarizable AMOEBA force field and *ab initio* molecular dynamics, *J. Phys. Chem. B* **124**, 3568 (2020).
- [4] P. Montero de Hijes, C. Dellago, R. Jinnouchi, and G. Kresse, Density isobar of water and melting temperature of ice: Assessing common density functionals, *J. Chem. Phys.* **161**, 131102 (2024).
- [5] N. O'Neill, B. X. Shi, K. Fong, A. Michaelides, and C. Schran, To pair or not to pair? Machine-learned explicitly-correlated electronic structure for NaCl in water, *J. Phys. Chem. Lett.* **15**, 6081 (2024).
- [6] P. R. Nagy, G. Samu, and M. Kállay, An integral-direct linear-scaling second-order Møller–Plesset approach, *J. Chem. Theory Comput.* **12**, 4897 (2016).
- [7] P. B. Szabó, J. Csóka, M. Kállay, and P. R. Nagy, Linear-scaling open-shell MP2 approach: Algorithm, benchmarks, and large-scale applications, *J. Chem. Theory Comput.* **17**, 2886 (2021).
- [8] P. R. Nagy, G. Samu, and M. Kállay, Optimization of the linear-scaling local natural orbital CCSD(T) method: Improved algorithm and benchmark applications, *J. Chem. Theory Comput.* **14**, 4193 (2018).
- [9] L. Gyevi-Nagy, M. Kállay, and P. R. Nagy, Integral-direct and parallel implementation of the CCSD(T) method: Algorithmic developments and large-scale applications, *J. Chem. Theory Comput.* **16**, 366 (2020).
- [10] M. Kállay, P. R. Nagy, D. Mester, Z. Rolik, G. Samu, J. Csontos, J. Csóka, P. B. Szabó, L. Gyevi-Nagy, B. Hégyel, I. Ladjászki, L. Szegedy, B. Ladóczki, K. Petrov, M. Farkas, P. D. Mezei, and Á. Ganyecz, The MRCC program system: Accurate quantum chemistry from water to proteins, *J. Chem. Phys.* **152**, 074107 (2020).
- [11] K. A. Peterson and T. H. Dunning, Jr., Accurate correlation consistent basis sets for molecular core–valence correlation effects: The second row atoms Al–Ar, and the first row atoms B–Ne revisited, *J. Chem. Phys.* **117**, 10548 (2002).
- [12] N. B. Balabanov and K. A. Peterson, Systematically convergent basis sets for transition metals. I. All-electron correlation consistent basis sets for the 3d elements Sc–Zn, *J. Chem. Phys.* **123**, 064107 (2005).
- [13] F. Weigend, M. Häser, H. Patzelt, and R. Ahlrichs, RI-MP2: Optimized auxiliary basis sets and demonstration of efficiency, *Chem. Phys. Lett.* **294**, 143 (1998).

- [14] A. Hellweg, C. Hättig, S. Höfener, and W. Klopper, Optimized accurate auxiliary basis sets for RI-MP2 and RI-CC2 calculations for the atoms Rb to Rn, *Theor. Chem. Acc.* **117**, 587 (2007).
- [15] G. L. Stoychev, A. A. Auer, and F. Neese, Automatic generation of auxiliary basis sets, *J. Chem. Theory Comput.* **13**, 554 (2017).
- [16] S. Lehtola, Straightforward and accurate automatic auxiliary basis set generation for molecular calculations with atomic orbital basis sets, *J. Chem. Theory Comput.* **17**, 6886 (2021).
- [17] F. Neese and E. F. Valeev, Revisiting the atomic natural orbital approach for basis sets: Robust systematic basis sets for explicitly correlated and conventional correlated ab initio methods?, *J. Chem. Theory Comput.* **7**, 33 (2011).
- [18] V. Blum, R. Gehrke, F. Hanke, P. Havu, V. Havu, X. Ren, K. Reuter, and M. Scheffler, Ab Initio molecular simulations with numeric atom-centered orbitals, *Comput. Phys. Commun.* **180**, 2175 (2009).
- [19] S. Grimme, J. Antony, S. Ehrlich, and H. Krieg, A consistent and accurate ab initio parametrization of density functional dispersion correction (DFT-D) for the 94 elements H-Pu, *J. Chem. Phys.* **132**, 154104 (2010).
- [20] T. D. Kühne, M. Iannuzzi, M. Del Ben, V. V. Rybkin, P. Seewald, F. Stein, T. Laino, R. Z. Khaliullin, O. Schütt, F. Schiffmann, D. Golze, J. Wilhelm, S. Chulkov, M. H. Bani-Hashemian, V. Weber, U. Borštnik, M. TAILLEFUMIER, A. S. Jakobovits, A. Lazzaro, H. Pabst, T. Müller, R. Schade, M. Guidon, S. Andermatt, N. Holmberg, G. K. Schenter, A. Hehn, A. Bussy, F. Belleflamme, G. Tabacchi, A. Glöß, M. Lass, I. Bethune, C. J. Mundy, C. Plessl, M. Watkins, J. VandeVondele, M. Krack, and J. Hutter, CP2K: An electronic structure and molecular dynamics software package - Quickstep: Efficient and accurate electronic structure calculations, *J. Chem. Phys.* **152**, 194103 (2020).
- [21] S. Goedecker, M. Teter, and J. Hutter, Separable dual-space Gaussian pseudopotentials, *Phys. Rev. B* **54**, 1703 (1996).
- [22] M. Guidon, J. Hutter, and J. VandeVondele, Auxiliary density matrix methods for Hartree-Fock exchange calculations, *J. Chem. Theory Comput.* **6**, 2348 (2010).
- [23] A. Bussy, O. Schütt, and J. Hutter, Sparse tensor based nuclear gradients for periodic Hartree-Fock and low-scaling correlated wave function methods in the CP2K software package: A massively parallel and GPU accelerated implementation, *J. Chem. Phys.* **158**, 164109 (2023).
- [24] H.-Z. Ye and T. C. Berkelbach, Correlation-consistent Gaussian basis sets for solids made simple, *J. Chem. Theory Comput.* **18**, 1595 (2022).

- [25] K. R. Bryenton, A. A. Adeleke, S. G. Dale, and E. R. Johnson, Delocalization error: The greatest outstanding challenge in density-functional theory, *Wiley Interdiscip. Rev.:Comput. Mol. Sci.* **13**, e1631 (2023).
- [26] J. Cheng, X. Liu, J. VandeVondele, M. Sulpizi, and M. Sprik, Redox potentials and acidity constants from density functional theory based molecular dynamics, *Acc. Chem. Res.* **47**, 3522 (2014).
- [27] M. Yu and D. R. Trinkle, Accurate and efficient algorithm for Bader charge integration, *J. Chem. Phys.* **134**, 064111 (2011).
- [28] A. P. Thompson, H. M. Aktulga, R. Berger, D. S. Bolintineanu, W. M. Brown, P. S. Crozier, P. J. in 't Veld, A. Kohlmeyer, S. G. Moore, T. D. Nguyen, R. Shan, M. J. Stevens, J. Tranchida, C. Trott, and S. J. Plimpton, LAMMPS - A flexible simulation tool for particle-based materials modeling at the atomic, meso, and continuum scales, *Comput. Phys. Commun.* **271**, 108171 (2022).
- [29] M. Bonomi, G. Bussi, C. Camilloni, G. A. Tribello, P. Banáš, A. Barducci, M. Bernetti, P. G. Bolhuis, S. Bottaro, D. Branduardi, R. Capelli, P. Carloni, M. Ceriotti, A. Cesari, H. Chen, W. Chen, F. Colizzi, S. De, M. De La Pierre, D. Donadio, V. Drobot, B. Ensing, A. L. Ferguson, M. Filizola, J. S. Fraser, H. Fu, P. Gasparotto, F. L. Gervasio, F. Giberti, A. Gil-Ley, T. Giorgino, G. T. Heller, G. M. Hocky, M. Iannuzzi, M. Invernizzi, K. E. Jelfs, A. Jussupow, E. Kirilin, A. Laio, V. Limongelli, K. Lindorff-Larsen, T. Löhr, F. Marinelli, L. Martin-Samos, M. Masetti, R. Meyer, A. Michaelides, C. Molteni, T. Morishita, M. Nava, C. Paissoni, E. Papaleo, M. Parrinello, J. Pfaendtner, P. Piaggi, G. Piccini, A. Pietropaolo, F. Pietrucci, S. Pipolo, D. Provasi, D. Quigley, P. Raiteri, S. Raniolo, J. Rydzewski, M. Salvalaglio, G. C. Sosso, V. Spiwok, J. Šponer, D. W. H. Swenson, P. Tiwary, O. Valsson, M. Vendruscolo, G. A. Voth, A. White, and The PLUMED consortium, Promoting transparency and reproducibility in enhanced molecular simulations, *Nat. Methods* **16**, 670 (2019).
- [30] W. C. Witt, Symmetrix, available at: <https://github.com/wcwitt/symmetrix> (2026).
- [31] D. P. Kovács, I. Batatia, E. S. Arany, and G. Csányi, Evaluation of the MACE force field architecture: From medicinal chemistry to materials science, *J. Chem. Phys.* **159**, 044118 (2023).
- [32] B. Armstrong, A. Silvestri, R. Demichelis, P. Raiteri, and J. D. Gale, Solubility-consistent force field simulations for aqueous metal carbonate systems using graphical processing units, *Philos. Trans. R. Soc., A* **381**, 20220250 (2023).
- [33] J. Aufort, P. Raiteri, and J. D. Gale, Computational insights into Mg<sup>2+</sup> dehydration in the presence of carbonate, *ACS Earth Space Chem.* **6**, 733 (2022).
- [34] M. Invernizzi and M. Parrinello, Rethinking metadynamics: From bias potentials to probability

- distributions, *J. Phys. Chem. Lett.* **11**, 2731 (2020).
- [35] T. Morawietz, A. Singraber, C. Dellago, and J. Behler, How van der Waals interactions determine the unique properties of water, *Proc. Natl. Acad. Sci. U. S. A.* **113**, 8368 (2016).
- [36] K. Cai, C. Zhang, and X. Wu, Simulations of dielectric permittivity of water by machine learned potentials with long-range Coulombic interactions, *J. Chem. Phys.* **163**, 184503 (2025).
- [37] Y. Wu, H. L. Tepper, and G. A. Voth, Flexible simple point-charge water model with improved liquid-state properties, *J. Chem. Phys.* **124**, 024503 (2006).
- [38] J. W. Ponder, C. Wu, P. Ren, V. S. Pande, J. D. Chodera, M. J. Schnieders, I. Haque, D. L. Mobley, D. S. Lambrecht, R. A. J. DiStasio, M. Head-Gordon, G. N. I. Clark, M. E. Johnson, and T. Head-Gordon, Current status of the AMOEBA polarizable force field, *J. Phys. Chem. B* **114**, 2549 (2010).
- [39] M. Invernizzi and M. Parrinello, Exploration vs convergence speed in adaptive-bias enhanced sampling, *J. Chem. Theory Comput.* **18**, 3988 (2022).
- [40] J.-N. Boyn and E. A. Carter, Characterizing the mechanisms of Ca and Mg carbonate ion-pair formation with multi-level molecular dynamics/quantum mechanics simulations, *J. Phys. Chem. B* **127**, 10824 (2023).